FILM BOILING OF SATURATED LIQUID FLOWING UPWARD THROUGH A HEATED TUBE: HIGH VAPOR QUALITY RANGE

WILLIAM F. LAVERTY
WARREN M. ROHSENOW

SEPTEMBER 1964

NSF CONTRACT GP-1245
REPORT NO. 9857-32

DEPARTMENT OF MECHANICAL ENGINEERING
MASSACHUSETTS INSTITUTE OF TECHNOLOGY

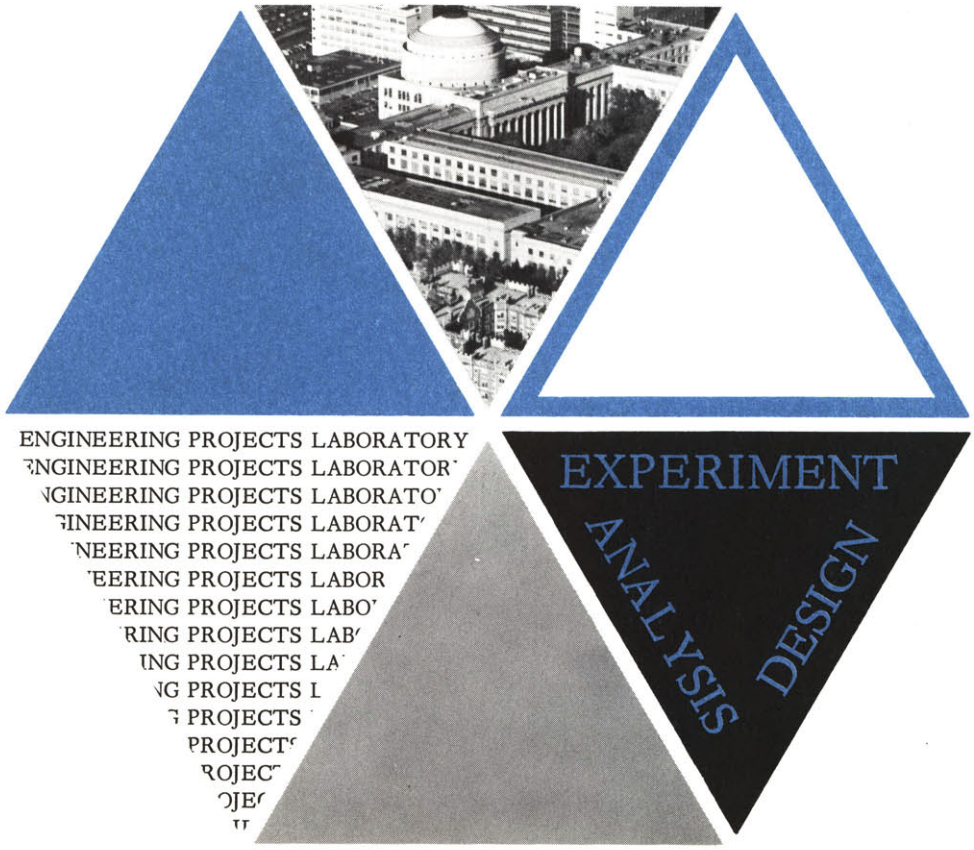

TECHNICAL REPORT NO. 9857-32

FILM BOILING OF SATURATED LIQUID FLOWING UPWARD THROUGH A HEATED TUBE: HIGH VAPOR QUALITY RANGE

by

WILLIAM F. LAVERTY
WARREN M. ROHSENOW

Sponsored by the
National Science Foundation
Contract No. NSF GP-1245

Department of Mechanical Engineering
Massachusetts Institute of Technology
Cambridge 39, Massachusetts

ABSTRACT

Film boiling of saturated liquid flowing upward through a uniformly heated tube has been studied for the case in which pure saturated liquid enters the tube and nearly saturated vapor is discharged. Since a previous study at the M.I.T. Heat Transfer Laboratory covered the case in which only a small percentage of the total mass flow is vaporized, this investigation has been concentrated on film boiling in the region where the vapor quality is greater than 10 percent.

Visual studies of film boiling of liquid nitrogen flowing through an electrically conducting pyrex tube have been made to determine the characteristics of the two-phase flow regimes which occur as a result of the film boiling process. It was found that the annular flow regime with liquid in the core and vapor between the liquid and the tube wall, which exists at very low qualities, is broken up at higher qualities to form a dispersed flow of droplets and filaments of liquid carried along in a vapor matrix.

A stainless steel test section having a .319 inch ID and heated electrically, has been used to obtain experimental data of wall temperature distributions along the tube and local heat transfer coefficients for different heat fluxes and flow rates with liquid nitrogen as the test fluid. Heat flux has been varied from 3500 to 30000 BTU/hr-ft^2 and mass velocity from 70000 to 210000 lbm/hr-ft^2. From these tests, values of wall superheat, $(T_w - T_s)$, from 200 to 975°F and heat transfer coefficients from 11.1 to 65.5 BTU/hr-ft^2-°F have been obtained.

A theoretical derivation using the Dittus-Boelter equation as an asymptote for the heat transfer to pure vapor has demonstrated that a significant amount of vapor superheat is present throughout the film boiling process. The mechanism of the heat transfer process in the dispersed flow region has been described by a two step theory in which 1) all of the heat from the wall is transferred to the vapor and 2) heat is transferred from the vapor to the liquid drops. A method has been given by which both an upper bound of the heat transfer coefficient to the dispersed flow and an estimate of its true value may be calculated.

ACKNOWLEDGMENTS

Financial support for this investigation was supplied by a grant from the National Science Foundation.

The authors are indebted to Professor S. C. Collins, Professor J. L. Smith and the staff of the Cryogenic Engineering Laboratory for their continued support throughout the experimental program.

TABLE OF CONTENTS

TABLE OF CONTENTS (Continued)

TABLE OF FIGURES

TABLE OF FIGURES (Continued)

I. INTRODUCTION

Purpose of the Investigation

The heat transfer process known as film boiling occurs when the wall confining a liquid is at a temperature much greater than the saturation temperature of the liquid. When this condition exists the rate of generation of vapor is so great that a vapor layer, or film, forms between the wall and the liquid. Once established, the film acts as a barrier to the flow of heat and allows a large temperature difference to exist while only a moderate heat flux passes from wall to liquid. Recent advances in the high temperature strength of materials and applications of cryogenic fluids as coolants have created a need for greater understanding of the film boiling process. Typical examples of the occurance of film boiling are found in the cooling of rocket engines, the quenching of metals and in transient temperature fluctuation of liquid cooled magnets and nuclear reactors upon loss of coolant flow.

As shown in the literature review, previous investigations of film boiling have been limited to heat transfer from heated surfaces suspended in a stagnant pool and to forced convection film boiling where the vapor fraction was small. In view of this, the intent here is to extend the knowledge of the case of forced convection film boiling in which large vapor fractions are generated in an enclosed passage. Previous studies of film boiling at the MIT

Heat Transfer Laboratory have dealt with film boiling at low vapor fractions of saturated liquid flowing through a uniformly heated tube. As a result, the extension of the same configuration to include higher vapor qualities has provided the specific objective: to experimentally investigate the mechanism of film boiling heat transfer of saturated liquid flowing upward through a uniformly heated tube for the case in which most of the liquid is evaporated.

Scope of the Research

Employing liquid nitrogen as a test fluid in tubes heated electrically by alternating current, two experimental programs were undertaken. The objective of the first of these was to determine qualitatively the characteristics of the two-phase flow regimes which occur as a result of the film boiling process. Using a four foot long, .417 inch inside diameter pyrex tube, internally coated with an electrically conducting transparent film, photographs were taken of the flow regimes along the entire length of the tube for the the following conditions:

Mass Flow Rate:	$\cong$	75000 lbm/hr-ft^2
Heat Flux:	$\cong$	10000 BTU/hr-ft^2
Pressure:	$\cong$	1.2 atm. absolute
Inlet Temperature:	$\cong$	-318 degrees F (saturation temperature)
Inlet Quality:	=	0

Following these tests a second series was undertaken to determine, quantitatively, the film boiling heat transfer coefficient. A 304

stainless steel test section having an inside diameter of .319 inches, an outside diameter of .375 inches and a 47.8 inch length (L/D=150), was instrumented with thermocouples to measure wall temperature over the following range of variables:

Mass Flow Rate	=	70000 to 210,000 lbm/hr-ft^2
Heat Flux	=	3500 to 30000 BTU/hr-ft^2
Wall Temperature	=	-120 to 650 degrees F
Pressure	$\cong$	1.2 atm absolute
Inlet Temperature	$\cong$	-318 degrees F (saturation temperature)
Inlet Quality	=	0

Analysis of the experimental data proceeded to demonstrate the mechanisms through which heat is carried to the two-phase mixture and by which evaporation of the liquid takes place. While it had originally been planned to correlate the data so that the film boiling heat transfer coefficients could be predicted, the results of the analysis show that a non-equilibrium condition exists between the liquid and vapor phases which precludes the success of such a correlation.

Literature Review

Beginning with the work of Bromley (1)*, dealing with film boiling in natural convection from a horizontal tube suspended in saturated liquid, there have been numerous studies of film boiling

*refers to Bibliography at the end of the paper.

from surfaces immersed in pools of liquid with both free and forced convection. Although Bromley succeeded in drawing an analogy between film boiling and film condensation such that his boiling data correlated well using a modified form of the Colburn equation for film condensation, the later analyses of McFadden and Gross (2) and of Koh (3) using vertical plates showed that, unlike condensation, the shear stress at the liquid vapor interface becomes important when there is any appreciable film velocity.

Aside from the very preliminary work of Carter (4), the subject of film boiling with forced convection inside of enclosed channels at low vapor fractions had not entered the literature prior to the beginning of the current series of film boiling studies at the MIT Heat Transfer Laboratory. The first of these, the work of R.A. Kruger (5), dealt with film boiling of saturated liquid flowing through a uniformly heated horizontal tube. His visual observation of film boiling of Freon 113 in a transparent, electrically conducting pyrex tube showed that vapor formed a thin film between the liquid core and the tube wall in the lower part of the tube and collected by circumferential flow into a vapor layer at the top of the tube. Using a model equivalent to the inverse of Bromley's for the thin film portion, and the Dittus-Boelter single phase, turbulent flow correlation for the heat transfer to the vapor layer at the top of the tube, he developed a theory to predict tube wall temperature distribution which agreed well with his experimental measurements. Following completion of Kruger's work, an extension of the same

subject to include the effect of subcooled liquid at the inlet was made by E.F. Doyle (6). Failure of a theory similar to that of Kruger to agree with the experimental data was attributed to transition rather than turbulent flow in the vapor layer at the top of the tube. It was shown that the experimental data was bracketed by assuming this vapor flow to be laminar on the one hand or turbulent on the other.

Reorientation of Kruger's problem to the vertical with upward flow, provided the subject of the third investigation which was undertaken by R.S. Dougall (7). Limiting his study to film boiling of saturated liquid at low vapor fractions, Dougall found through visual observation that the flow assumed an annular configuration with liquid flowing up the center in a core and vapor flowing upward in a generally thin film between the tube wall and a rather rough liquid vapor interface. Assuming the film to be turbulent and thin but of uniform thickness, he developed a theory for the heat transfer which predicted the tube wall temperature distribution with length and agreed relatively well with the experimental data. This theory did not show any effect of mass flow rate on the heat transfer coefficient and none was observed in the experimental data in the range of flow rated tested (5×10^5 to 8×10^5 lbm/hr-ft^2). An asymptote of the data at higher vapor fractions seemed to be given by the Dittus-Boelter equation with properties evaluated for saturated vapor and Reynold's number based on volume velocity. Since the present investigation covers the range of Dougall's study as an

initial condition, it was hoped that the above theory would be substantiated by the new experimental data.

A second correlation developed for film boiling in vertical tubes is that presented for hydrogen by Hendricks et al (8) which makes use of the Martinelli two-phase flow parameter in a correction to the Dittus-Boelter equation. Its agreement with their data was only approximate and an attempt by Dougall to use it in correlating his data failed both in magnitude and direction.

The investigation of Lewis et al (9), Parker and Grosh (10), Lavin and Young (11) and Polomik et al (12) dealt with film boiling in tubes after a considerable length of nucleate boiling. These publications contain a wealth of information applicable to the present problem but perhaps the remarks of Parker and Grosh concerning the decreased rate of evaporation of droplets once a spheroidal, or stable film boiling, condition is established are most significant. The initial length of nucleate boiling is certain to produce a condition of drops suspended in nearly saturated vapor at the onset of film boiling whereas an equivalent length of film boiling is likely to result in considerable vapor superheat since this superheat is the primary driving force for evaporation in the film boiling process. Thus the heat transfer coefficients obtained for film boiling at high vapor fraction with different initial evaporation mechanisms are likely to differ dramatically.

II. EXPERIMENTAL APPARATUS AND PROCEDURE

The experimental apparatus may be divided into the following subsystems:

1. General flow control components and instrumentation
2. Power circuit and instrumentation
3. Visual test section and photographic equipment
4. Quantitative test section and instrumentation
5. Vacuum Insulation System

A schematic diagram of the apparatus is shown in Figure 2.

General Flow Control Components and Instrumentation

The test apparatus is a once through boiler which is supplied by liquid nitrogen in a standard 50 liter metal dewar. The pumping head is obtained by pressurization of the dewar with helium from a gas cylinder regulated to approximately 15 psig. Since the nitrogen, as supplied in the dewar, is vented to the atmosphere and, therefore, at the saturation temperature corresponding to the barometric pressure, the use of helium as the pressurizing medium insures that the liquid supply temperature will remain at his value during blow-down of the dewar except for the small heat leakage through the container walls and the also small thermal energy carried in the pressurizing helium. The solubility of helium in liquid nitrogen is sufficiently small to preclude the possibility of significant quantities of helium being carried into the test section in the test fluid.

Liquid nitrogen is carried from the bottom of the dewar to the vacuum chamber which encloses and thermally isolates the test section and flash cooler, in 3/8 inch OD copper tube which is connected to the apparatus by a flare fitting. This fitting and the stainless steel tubes which are sealed to the supply tube on both sides of it, are insulated by Santocel powder contained by a removable jacket. This system thus provides an insulated connection which is easily broken each time the dewar needs refilling.

From the flare fitting, the supply tube passes through a Swagelok compression fitting which serves as a vacuum seal, into the vacuum chamber. Inside, the liquid nitrogen is fed to a valve at which a small part of the stream is bled off to supply the flash cooler. This cooler is a five foot long, concentric tube, parallel flow heat exchanger in which the main nitrogen supply flows in the center tube and the bleed flow, regulated by the bleed valve, flows in the annulus between the tubes. Both tubes are type L copper water tubing, the smaller having a 3/8 inch OD and the larger a 1/2 inch OD. The heat exchanger was coiled to fit in space 3½ inches in diameter by about 14 inches long. From the downstream end of the cooler, the bleed flow is carried outside the vacuum chamber to a pressure control valve and then through a steam heater (see pg.11) to the intake of a Welch 1397B mechanical vacuum pump. The pressure in the annulus of the cooler is measured by a bourdon vacuum gauge connected into the bleed line just upstream of the pressure control valve.

Following the flash cooler the main nitrogen supply passes through the flow control valve and through a length of tubing into the test section. The flow control valve is a Veeco R-38-S bellows-sealed brass angle valve modified with an extended stem to permit flow adjustments to be made manually outside the vacuum chamber. Since the pressure in the test section is only about 2 psig and the nitrogen supply pressure is about 15 psig, the pressure drop across the flow control valve is sufficient to prevent small pressure fluctuations in the test section from causing inlet flow oscillations. The 3 inch long test section inlet tube is soldered directly into the valve. It is a .375 inch OD, .319 inch ID, 304 stainless steel tube in which a static pressure tap is located at the midpoint and to which is cemented a thermocouple to measure nitrogen inlet temperature. The pressure tap is connected to two 24 inch mercury manometers outside the vacuum chamber, one of which reads inlet gauge pressure and the other, test section pressure drop. The helium pressure line is joined through a needle valve to the connecting tubing of the pressure tap so that air, which would liquefy in the lines, may be bled out.

On the end of the inlet tubing is silver-soldered a 303 stainless steel flange having a 1-3/4 inch OD and a .319 inch ID. This flange is bolted to a matching flange at the end of the test section with a 1/4 inch thick, 1 inch OD by .319 inch ID micarta spacer between them. Between each flange and the spacer, a number 17 Viton A O-ring is

crushed to .015 inches thickness by tightening the six stainless steel bolts. Since high voltages are applied across the test section, an interlocking system of micarta spacers is used to provide at least a 1/4 inch gap between the bolts and the inlet tube and flange at all points.

At the top of the test section a set of flanges identical to those at the bottom is used to join the test section to the discharge tube. Since the discharge tube also serves as the top electrode, no micarta is used at this connection, only one Viton A O-ring (crushed to .015 inches) is required and six brass bolts replace the stainless steel bolts used at the bottom. The discharge tube, a 1/2 inch OD type K copper water tube, passes out of the vacuum chamber through another Swagelok compression fitting seal, makes connection with the upper power cable and extends into a nylon Swagelok union which electrically insulates it from the piping downstream. The Swagelok vacuum seal is connected to the top of the vacuum chamber by a brass bellows which allows the test section to expand and contract freely.

In order to measure the nitrogen flow rate in a standard rotameter it is necessary to heat the discharge from the apparatus to near room temperature. Two independently controlled steam heat exchangers were put in the flow line for this purpose, one 5 feet long and the other 8 feet long. Between the nylon union and the first heat exchanger, a second bellows expansion joint was installed to take up thermal expansion and a second pressure tap was drilled to obtain the test section pressure drop. Both heat exchangers are tube-in-tube types

made up from type L copper water tubing and sweat fittings. The inner tube has a 7/8 inch OD and the outer tube a 1-1/8 inch OD. In both cases the steam passes through the annulus and the nitrogen through the center tube. The exhaust steam is collected in a single 1/2 inch OD copper tube, passed through the flash cooler bleed line heater and condensed in a drain line by a stream of water. The flash cooler bleed line heater is a tube-in-tube heat exchanger in which the steam exhaust line is the center tube. The outer tube is a 7/8 inch OD copper water tube, 3 feet long, and the bleed flow passes through the annulus.

Between the second steam heater and the flow meter is a three foot length of 3/4 inch brass pipe in the middle of which is a pressure tap connected directly to bourdon pressure gauge. A thermometer set in a 1/4 inch Conax packing gland is used to measure gas temperature at the flow meter inlet. The flow meter itself is a Brooks Model 10-1110 Rotameter calibrated to 1% of full scale (250 mm = 118 lbm/hr of N_2 at $70^{\circ}F$ and 14.7 psia). Following the flow meter the nitrogen passes through a pressure control valve and is exhausted to the atmosphere.

Power Circuit and Instrumentation

The 115 volt, 60 cycle alternating current laboratory power is used as the power source for heating the test section. It has a 3kw capability, sufficient to produce a bulk quality of 1.0 at the test section exit (saturated liquid at the inlet) over the

entire range of flow rates studied. A 5 KVA Variac variable transformer which can convert the 115 volt supply to from 0 to 135 volts, is used to control the test section power. Since the visual test section has an electrical resistance of approximately 380 ohms while the quantitative test section has a resistance of only about .04 ohms, two different transformers were required to convert the Variac output to voltages compatible with the test section resistance and power dissipation requirements. The transformer used with the visual test section is a Westinghouse Type CSP single phase transformer having a 7.5 KVA rating and wired to boost the input voltage by a factor of 10. The one used with the quantitative test section is a GE Boost and Buck transformer Model 9T51Y113 which has a rating of 3 KVA and was wired to reduce the input voltage by a factor of 10.

The power input to the test section, in both cases, was measured by current and voltage readings from a-c meters. For the visual test section, a Model 59 Simpson voltmeter with external multiplier giving it a range of 0 to 1000 volts and a Model 59 Simpson ammeter with a range of 0 to 3 amps were used. Since the current was small and line losses were negligible for the visual set up, the voltmeter was located with the ammeter on the high voltage transformer enclosure and the voltage taps were made close to the transformer. The meters used with the quantitative test section were a Model 115 Weston ammeter with a range of 0 to 250 amps and a Model 433 Weston voltmeter with a 0 to 10 volts, 0 to 20 volts dual range. Both of these latter instruments were calibrated to give $\pm$ 1/2% of full scale accuracy.

Since the line losses were appreciable, the voltmeter taps were made at the discharge tube at the top of the vacuum chamber and at the external end of the Conax electrode gland.

Two different sets of power cables were used to carry the power to the apparatus for the two test sections. The cables used for the visual test section are No. 14, 15 KV rated wire while those used for the quantitative test section are 3/0 welding cable. The connection at the top of the test section was made by connecting the cable to a brass clamp which is bolted tightly around the nitrogen discharge tube. At the lower end a Conax electrode gland, No. EG-31-Cu-L type A, was employed to carry the power inside the vacuum chamber. When used with the high voltage power supply, the exposed end connections of the gland were covered completely with electrical tape as a safety precaution. Inside the chamber two different arrangements were used to connect the gland to the lower flange of the test section. For the visual test section it was sufficient to simply run a short length of high voltage wire from the gland to one of the stainless steel flange bolts, using an extra nut to faster it in place. For the quantitative test section a 1 inch by 1/16 inch copper strip was used to connect the gland to a 1/8 inch thick, U-shaped plate which was bolted down against the flange nuts by six additional nuts. In order to measure the heat conduction loss through the buss, two thermocouples were attached to the copper strip 1 inch apart. The outer one was

wired to read the buss temperature and the inner one was wired to read the temperature difference between them.

Visual Test Section and Photographic Equipment

As mentioned previously the visual test section is a pyrex tube internally coated with a transparent electrically conducting coating. It has a .512 inch OD and a .417 inch ID and is joined to end flanges by graded glass, pyrex to kovar, seals and 1 inch lengths of kovar tubing copper-gold soldered to the flanges. The E-C coating which forms a 45.9 inch heated length was applied by the Corning Glass Works on an experimental basis. A layer of silver fired onto the tube makes the electrical contact between the coating and the end flanges. Since the coating is limited to a maximum operating temperature of 660^{o}F, one thermocouple was attached to the outside of the tube about six inches from the test section to monitor tube temperature. Thermal isolation of the test section, except for small end losses and radiation losses, was provided by vacuum insulation as is discussed more fully on page 16. In order to see the test section and make visual studies, the portion of the vacuum chamber surrounding the test section was made from a transparent lucite tube.

Flow regime photographs were taken with a Polaroid Model 110B camera using close-up lens' which give a 3 inch by 4 inch field at a focal distance of 6 inches. The film used was Polaroid Type 47 (ASA 3000) and the lighting was provided by a General Radio Type

1530-A Microflash which was tripped by the camera shutter. For easy adjustment of camera position anywhere along the test section, a tubular "unipod" was built along which a camera support arm can be slid and clamped to give the desired field.

Quantitative Test Section and Instrumentation

The quantitative test section is a .375 inch OD, .319 inch ID 304 stainless steel seamless tube which is 47.8 inches long. At each end a 303 stainless steel flange is silver soldered to it for connection with the inlet and discharge piping (see page 9). Fifteen copper-constantan thermocouples are cemented with magnet wire varnish to its external surface at approximately 3 inch intervals (see Table I). These thermocouples were made up from 30 gauge glass wrapped duplex wire and were calibrated over the range of operating temperatures. A thin (.002 inch) piece of mica is imbedded in the cement under the bare end of each thermocouple junction in order to electrically insulate it from the test section. In addition, approximately the last inch of wire before each junction is cemented to the tube wall to provide a heat sink for the lead wire without inducing thermocouple errors. An aluminum foil radiation shield, separated from the tube by a layer of asbestos cloth tape and cut to fit around the thermocouple lead wires, is wrapped around the test section to reduce the radiation loss from the test section and thermocouple junctions. This entire unit is enclosed in the vacuum chamber to eliminate convection losses to the surroundings.

The constantan wires from the fifteen test section thermocouples, the inlet tube thermocouple and the buss bar temperature thermocouple were soldered together inside the vacuum chamber and one 24 gauge constantan wire was run from this junction through a pass-through tube to an ice junction outside the vacuum chamber. Each of the copper wires from the above thermocouples plus the one from the temperature difference thermocouple on the buss bar was run through its own pass through tube to the outside. The fifteen test section thermocouples and the inlet temperature thermocouple were then wired up so that they could either be read on a 16 channel Brown recorder (Minneapolis-Honeywell Model 153X62V16) or by a potentiometer or millivoltmeter. The two buss bar thermocouples were wired to be read on the potentiometer or millivoltmeter only. The recorder has a range of 0 to 10 millivolts and was wired so that negative potentials could be read simply by flipping a switch. For the few runs in which wall temperatures occurred which produced thermocouple emf's greater than 10 millivolts, a constant measured emf was added into the circuit to convert the recorder range to slightly higher values (e.g. 5 to 15 mv).

Vacuum Insulation System

The vacuum chamber consists of two sections. The lower section which contains the flash cooler and flow control valve, is a 5 inch OD brass tube, 18 inches long with 1/2 inch thick brass end plates. Through the bottom plate which is soldered to the brass tube, pass

the enclosed flow control valve stem, sealed by a neoprene O-ring and the nitrogen supply tube, sealed by a Swagelok compression fitting at the bottom end of a six inch stainless steel extension tube. The top plate is bolted to a flange on the brass tube and sealed by a neoprene O-ring. The bleed flow line and enclosed bleed valve stem pass through the top plate and are sealed by Swagelok compression fittings. The Conax electrode gland is also located in this plate as is the miniature Conax packing gland which seals the tube for the inlet flow pressure tap. A 1-3/8 inch OD copper tube which is silver soldered into the brass tube just below the flange, serves as the evacuation port for the vacuum chamber. It is connected through a 1 inch diaphagm valve and a liquid nitrogen cold trap to a second 1397B Welsh mechanical vacuum pump. On either side of the evacuation port are two electrical pass-throughs, each of which consists of 6 or 9 small electrically insulated vacuum tight tubes for thermocouple wires to pass through and be soldered to.

The upper section of the vacuum chamber is a four foot long, 3 inch OD, 2-1/2 inch ID lucite tube which is sealed at each end by neoprene O-rings. It is held between the top plate of the lower chamber and a 1/2 inch thick brass cover plate by four 1/4 inch diameter stainless steel rods. These rods are spring loaded at the top to permit thermal expansion of the lucite. Since the cover plate is in electrical contact with the top power cable it was necessary to insulate it from the lower section of the vacuum chamber. This was accomplished by wrapping each of the rods with several layers of

electrical tape in the region where they pass through the cover plate and by placing micarta washers under the springs.

Vacuum chamber pressure is sensed by a National Research Corporation Type 501 Thermocouple Gauge located in the evacuation line near the lower chamber. The control unit for the gauge is an NRC Type 701.

Experimental Procedure

Before hooking up a full dewar of liquid nitrogen the vacuum chamber is evacuated to a pressure of about 1 micron of mercury absolute and the entire flow system is flushed with prepurified nitrogen from a gas cylinder. With the dewar in place and pressurized and the steam heaters turned on, the apparatus is ready to operate. The first steam heater is set initially and then not changed since it is in danger of freezing up at low steam flow rates. Cool-down of the inlet piping proceeds by opening the flow control valve while at the same time adjusting the test section power to keep the test section wall temperature in the film boiling range. When the inlet temperature approaches saturation temperature, the bleed valve is cracked open to start the cold stream through the flash cooler. After the inlet flow reaches the pure liquid condition, the flow control valve, and back-pressure control valve are set to give the desired flow rate and system pressure, and the variac and second steam heater are set to give the desired test section heat flux and flow

meter inlet temperature. A small amount of helium is then bled into the lower pressure tap tube to purge the air from it and the system is ready for operation.

Although no provision was made for measuring the bleed flow rate and the copper constantan inlet temperature thermocouple is not sufficiently accurate to measure inlet subcooling, the operating procedure for the bleed system was easily established during visual testing by observing the bleed control settings at which vapor is just eliminated from the inlet flow. Since the heat flow into the dewar and lower chamber is independent of flow rate and test section heat flux, one setting was obtained which could be used throughout the testing. The bleed back-pressure valve was then left in this position and the bleed flow control valve was set each time to give a back-pressure of about 22 inches of mercury vacuum at the gauge. This resulted in a flash cooler cold stream temperature of about $120^{\circ}R$ and a nearly constant bleed flow rate.

For each visual run the following quantities were recorded: flow rate-mm, flow meter temperature-$^{\circ}F$, system back pressure-psig, test section current-amps and voltage-volts, inlet flow temperature-mv, test section reference temperature-mv, bleed pressure-inches Hg vacuum and photograph numbers and positions. Preliminary testing proved that backlighting, obtained by bouncing the Microflash light off a white background, was most effective in illuminating the flow patterns while avoiding reflections from the lucite and pyrex surfaces. At high vapor qualities, a white background with a black center

directly behind the portion of the tube being photographed, was found to provide the better contrast needed to outline very small droplets. Figure 3 is a schematic plan view of photographic layout.

The quantitative data was taken for a range of heat fluxes at each of four flow rates, G $\cong$ 70000, 115000, 160000, 210000 lbm/hr-ft^2. The Brown recorder, which cycles through the 16 channels about once every 20 seconds, was used both to record the tube wall and inlet temperature and to establish when a run had reached equilibrium conditions. On the average it took about 10 minutes for a run to reach equilibrium and, as a result, from four to eight runs could be made on one 50 liter charge of nitrogen depending on the flow rate. Once the system reached equilibrium the following quantities were recorded manually: flow rate-mm, flow meter temperature-^{o}F, system back-pressure-psig, test section current-amps, and voltage-volts, test section inlet pressure and pressure drop-mmHg, bleed pressure-inches Hg vacuum, and lower buss temperature and temperature difference-mv. Two series of data runs were made in order to establish reproducibility.

III. DATA ANALYSIS, RESULTS AND DISCUSSION

Reduction of Experimental Data

For both the visual and quantitative tests the flow rate data was reduced to lbm/hr with the rotameter calibration curve and temperature and pressure correction curves. Flow meter inlet temperature and system back-pressure corrected to absolute pressure were used to evaluate the temperature and pressure correction factors respectively.

Since the visual studies were intended to be only qualitative in scope and the heat flux was relatively non-uniform, the average heat flux in BTU/hr-ft^2 was estimated using the equation:

$$\frac{Q}{A} = \frac{IE}{\pi D_w L_o} \tag{1}$$

and the local vapor quality was estimated by the equation:

$$X = 4\frac{Q}{A}\ \frac{1}{G h_{fg}}\ \frac{L}{D_w} \tag{2}$$

where h_{fg} was evaluated at the system back pressure.

The average heat flux for each of the quantitative test runs was computed using the equation:

$$\frac{Q}{A} = \frac{1}{\pi D_w L_o}\left(IE - I^2 R_{buss} - Q_{Loss}\right) \tag{3}$$

R_{buss} was estimated by the equation:

$$R_{buss} = 97.1\ in.^{-1}\ r_{buss}(T_{buss}) + 18.5\ \mu\Omega \qquad (4)$$

where the first term is the resistance of the lower buss between the lower voltage tap and the lower test section flange and the second term is the resistance of the discharge tube between the upper voltage tap and the upper test section flange. The I^2R_{buss} term was less than 0.3% of the IE product for all runs. Q_{loss}, the thermal loss from the outer surface of the test section, was taken from Figure 24 at the average test section wall temperature. It was less than 1.8% of the IE product for all runs. The thermal loss data for Figure 30 was obtained from no flow tests using the equation:

$$Q_{Loss} = \left(W_{TS}\, C_{P_{TS}} + W_I\, C_{P_I} \right) \frac{dT}{dt} \qquad (5)$$

where $W_{TS}\, C_{P_{TS}}$ is the heat capacity of the test section and $W_I\, C_{P_I}$ is the heat capacity of the asbestos insulation between the test section and the radiation shield.

Test section inlet pressure, P_i, was converted to absolute pressure in psia using the barometric pressure, and test section pressure drop, ΔP, was converted to psi. The pressure drop was found to be sufficiently small that the heat of vaporization, h_{fg}, varied no more than 1% in the length of the test section. Therefore h_{fg} was always evaluated at P_i.

Wall temperature values were obtained directly from the Brown recorder charts using the thermocouple calibration data. Bulk temperature of the nitrogen was taken as the saturation temperature of nitrogen at P_i for $L < L_{sat}$ where:

$$L_{sat} = \frac{G D_w h_{fg}}{4 \frac{Q}{A}} \tag{6}$$

For $L > L_{sat}$ the bulk temperature was taken to be the vapor temperature at a vapor enthalpy obtained from the equation:

$$H_v = H_{v_{sat}} + \frac{4 \frac{Q}{A} (L - L_{sat})}{G D_w} \tag{7}$$

The local heat transfer coefficient was then computed using the equation:

$$h_L = \frac{\frac{Q}{A}}{(T_w - T_b)_L} \frac{(r_{ss})_L}{(r_{ss})_{avg}} \tag{8}$$

where $(r_{ss})_L$ and $(r_{ss})_{avg}$ were taken from the solid line of Figure 25 at the local and average wall temperature respectively.

Nitrogen properties used in the data reduction were taken from references (13), (14) and (15). The resistivity of copper used in evaluating r_{bulk} was taken from reference (16). A tabulation of the quantitative data is given in Table II.

Visual Study

From the visual study it was determined that there are basically two flow regimes which occur. At the beginning of the heated section, where the vapor fraction is small, the flow is annular with the liquid in the center and the vapor in the annulus as shown by Figure 4a. Because of the large velocity increase caused by the generation of low density vapor, the drag force on the liquid core increases at greater tube lengths to the point that the core is torn apart into filaments and droplets of liquid. The beginning of this break-up is evident at the top of Figure 4b. As the break-up continues the flow goes through a somewhat gradual transition to a dispersed flow regime in which small droplets and filaments of liquid are carried along in a vapor matrix. Figures 5 and 6 illustrate the nature of the dispersed flow. In Figure 5 the decrease of average drop size with increasing length (and vapor quality) and a tendency of the largest liquid particles to be concentrated in the vapor boundary layer are both evident. Also noticeable in the progression from 5a to 5b is the characteristic of the particles to become more uniformly distributed at greater vapor qualities. Figure 6, taken with the dark background which tends to bring out the very small droplets at the sacrifice of obscuring the larger ones, is a duplicate of the conditions of Figure 5a. The two photographs were taken a few seconds apart and show the unsteady nature of the flow of the very small drops. This effect was easily seen by

the naked eye and is apparently due to periodic shattering of large liquid filaments in a region about ten inches from the start of the heated section.

Quantitative Study

Figures 7 to 11 summarize the results of the quantitative experimental program, showing wall superheat variation with heated length, heat flux and flow rate. For the lower flow rates the wall temperature rises from the inlet to a maximum value after which it decreases smoothly to a minimum. Both the maximum and the minimum are seen to move away from the inlet as heat flux is decreased and as flow rate is increased. By comparison of the visual results with the data of run 26 (Figure 7) which has approximately the same heat flux and mass velocity as that used in the visual tests, it was found that the maximum wall temperature corresponds to the transition to dispersed flow. Since both the vapor fraction and fluid acceleration at a given length decrease with decreasing heat flux or increasing mass velocity, the transition must at least shift in the same direction as does the temperature maximum. The secondary depression of wall temperature following the maximum for the highest level of flow rate (Figure 10) is not accountable but it is suggested that the initial breakup of the liquid core may occur suddenly at a critical liquid-vapor velocity difference or Weber number after which dispersion continues in the gradual manner found in the visual study.

In order to present the data in a more conventional form, the local heat transfer coefficients for typical runs at each flow rate, converted to Nusselt number, $\frac{h D_w}{k_{vf}}$, are shown in Figure 12. Although data points are not plotted for the sake of clarity the scatter from each line was no more than three percent. In Figure 13 some of these data are compared with the theory of Dougall (7). Since his experimental results showed no significant effect of either heat flux or flow rate upon Nusselt number in the low quality range there is no agreement between his theory and the nitrogen data. The most apparent cause of the discrepancy lies in the assumption used in the theory that the vapor annulus remains thin relative to the tube diameter. From the visual results it is quite evident that this is not the case in film boiling of liquid nitrogen. Why it should be valid for Freon 113 when it is not for nitrogen remains as yet an open question.

In order to understand the behavior of the wall temperature at higher vapor qualities it is well to consider the asymptote which is met when the evaporation is complete. If equilibrium were maintained between the two phases, this would occur at a length, L_{sat}, given by equation (6). Since over the range of flow rates studied the pure vapor state implies turbulent flow, we should be able to predict the wall temperature for $L > L_{sat}$ using a form of the Dittus-Boelter equation:

$$\frac{h D_w}{k_{vb}} = .023 \left(\frac{G D_w}{\mu_{vb}}\right)^{0.8} Pr_{vb}^{0.4} \tag{9}$$

For a high wall-to-fluid temperature ratio it has been suggested (e.g. ref. 17) that the fluid properties be evaluated at film temperature, $T_f = \frac{1}{2}(T_w + T_b)$, and that the velocity used in computing the Reynolds number be evaluated at the bulk temperature so that the equation becomes:

$$\frac{h D_w}{k_{vf}} = .023 \left(\frac{\rho_{vf} V_b D_w}{\mu_{vf}}\right)^{0.8} Pr_{vf}^{0.4} \tag{10}$$

Figure 14 is a comparison of wall temperatures of run 56 with those calculated by equations (9) and (10) assuming saturated vapor at length L_{sat} and the heat flux and mass velocity of run 56. The high values of wall temperature predicted by equation (10) at low vapor superheats is due to the rapid percentage increase of nitrogen vapor density, with corresponding decrease in bulk velocity, as saturation is approached. In the region in which equation (10) has been tested (e.g. ref. 18) the absolute temperature of the gas was much greater than that of saturated nitrogen and the correction resulting from the difference between equations (9) and (10) was only a shift of wall temperature level and not a change of curve shape. Since there is no known available data for heat transfer to cryogenic vapors in turbulent flow to confirm such a large temperature ratio

effect as that given by equation (10), it was decided that equation (9) provides a better estimate of the heat transfer coefficient for nearly saturated nitrogen vapor.

Two Step Heat Transfer Theory

Using equation (9) to compute the pure vapor asymptotes Figures 15 and 16 show the results of several runs at the lowest and highest flow rates with extrapolations showing approximately how they would approach their respective asymptotes if the heated test section were sufficiently long. On each run is indicated the point L_{sat}, at which the pure vapor state would have been attained had the vapor been in thermal equilibrium with the liquid (i.e. for $Tv=T_{sat}$). The fact that the data does not meet the asymptote at this length shows that a significant amount of superheat is present in the vapor and that the film boiling is not an equilibrium process. Therefore, as a model for the high quality, dispersed flow region of film boiling, it seems reasonable to assume that the heat transfer process may take place in two steps; first, from the wall to vapor at some temperature T_v, and second, from the vapor to the liquid. Since this implies that most all of the evaporation occurs outside the vapor boundary layer, the model will obviously be invalid for low qualities where the visual studies show there is a concentration of large liquid drops near the wall.

Heat Transfer to the Vapor

For the first step, assuming the vapor flow to be turbulent, the heat transfer may be calculated from a revised form of equation (9):

$$\frac{h_1 D_w}{k_v} = .023 \left[\frac{\rho_v D_w}{\mu_v} \left(\frac{q_v + q_\ell}{A_c} \right) \right]^{0.8} Pr_v^{0.4} \tag{11}$$

where the term $\frac{q_v + q_\ell}{A_c}$ is the through-put velocity and is calculated using the equation:

$$\frac{q_v + q_\ell}{A_c} = 4 \frac{Q}{A} \frac{L}{D_w (H_v - H_{\ell sat})} \left(\frac{1}{\rho_v} - \frac{1}{\rho_\ell} \right) + \frac{G}{\rho_\ell} \tag{12}$$

For the wall temperatures involved in the region of interest, the radiation emitted by the wall, assuming the wall to be black, amounts to no more than 5 percent of the total heat flux. Since the flow is dispersed, much of that energy strikes the tube wall elsewhere and is absorbed. Therefore radiation to the liquid is negligible and it follows that;

$$h_1 (T_w - T_b) = \frac{Q}{A} \tag{13}$$

The local heat flow for the second step is related to the first step by the heat balance:

$$\frac{Q_e}{\theta} = \frac{4}{D_w} \frac{Q}{A} - \frac{4 W_v C_p}{\pi D_w^2} \frac{dT_v}{dL} \tag{14}$$

where $\frac{Qe}{\vartheta}$ is the heat going into evaporation per unit volume of liquid-vapor mixture and W_v, the vapor flow rate is calculated using the heat balance:

$$w_v = \frac{\pi D_w L}{H_v - H_{\ell sat}} \frac{Q}{A} \tag{15}$$

Defining a volume evaporation coefficient, $ah_e = \frac{Qe}{\vartheta} / (T_v - T_s)$ equations (14) and (15) become:

$$ah_e = \frac{1}{T_v - T_s} \frac{4}{D_w} \frac{Q}{A} \left(1 - \frac{L C_p}{H_v - H_\ell} \frac{dT_v}{dL}\right) \tag{16}$$

where h_e is the mean evaporation heat transfer coefficient and a is the liquid surface area per unit volume of liquid-vapor mixture.

Limits of the Theory

Before proceeding with an analysis of the evaporation process of the second step, a check of the region of application of the theory is possible by computation of ah_e from the experimental data. When equations (11), (12) and (13) have been combined to form the equation:

$$\frac{\frac{Q}{A}}{T_w - T_v} = .023 \frac{k_v}{D_w} Pr_v^{0.4} \left[\frac{Q}{A} \frac{4L}{\mu_v (H_v - H_\ell)} \left(1 - \frac{\rho_v}{\rho_\ell}\right) + \frac{G D_w}{\mu_v} \frac{\rho_v}{\rho_\ell}\right]^{0.8} \tag{17}$$

it is evident that the vapor temperature can be found for each run at any length, L, simply by iteration. Figure 17 shows the calculated vapor temperature for a few typical runs. From plots like Figure 17, the slope, $\frac{dT_v}{dL}$, was measured at various values of L and equation (16) was solved for ah_e. Figure 18 shows the variation of ah_e with heated length for a portion of the test runs at each of the four flow rates. The left end of each line corresponds to a calculated vapor superheat of 20^oF. The rapid increase of ah_e at this end of the line indicates that significant amounts of liquid are in the boundary layer and, therefore, that the theory is invalid in this region. The figure shows that ah_e increases for higher mass velocities, increases slightly for higher heat fluxes and decreases slightly with length. For those runs which reached the highest vapor qualities it may be seen that ah_e starts to drop more rapidly near the end of the heated test section. The most plausible explanation of this slope change is that it marks the end of drop breakup and thus the end of a process which increases $\underline{a}$. As a final remark about Figure 18 it seems well to point out that ah_e must go to zero when the evaporation is complete since $\underline{a}$ must then be zero.

Evaporation of the Liquid

Both $\underline{a}$ and h_e depend on fluid properties, slip velocity and drop size. Because of the extremely complex nature of the breakup of the annular flow, the drop size spectrum is not something which

can be predicted by analysis of the fluid mechanics. Neither is it possible to experimentally measure the drop size, except as an order of magnitude estimate. For this reason, it is necessary to complete the analysis without the knowledge of drop size and to use the experimental data to provide the missing information.

Assuming that each drop is a sphere and knowing that the Prandtl number of nitrogen is about the same as air, the mean heat transfer coefficient, h_e, can be gotten from the following equation from McAdams (17):

$$\frac{h_e D_d}{k_{vi}} = .37 \left(\frac{\rho_{vi} \Delta V D_d}{\mu_{vi}} \right)^{0.6} \tag{18}$$

as long as the drop Reynolds number $\frac{\rho_{vi} \Delta V D_d}{\mu_{vi}}$, is greater than 17. Integrating over all drop sizes, $\underline{a}$ is given by the equation:

$$a = \int_0^\infty \pi D^2 N \, dD \tag{19}$$

where N is the concentration function for drop diameter. Similarly, the equation:

$$\frac{W_\ell}{\rho_\ell A_c V_\ell} = \int_0^\infty \frac{\pi}{6} D^3 N \, dD \tag{20}$$

is obtained by integrating the mass of all the drops contained in a unit volume of liquid-vapor mixture.

If the assumption is now made, that there is one equivalent drop diameter, D_s, which, when substituted for the real drop spectrum, will give the same resulting heat transfer, D_d can be replaced by D_s in equations (18), (19) and (20) with the result:

$$\frac{h_e D_s}{k_{vi}} = .37 \left(\frac{\rho_{vi} \Delta V D_s}{\mu_{vi}} \right)^{0.6} \tag{18a}$$

$$a = \pi D_s^2 n \tag{19a}$$

$$\frac{W_l}{\rho_l A_c V_l} = \frac{\pi}{6} D_s^3 n \tag{20a}$$

Combining these last three equations and solving for ah_e produces the equation:

$$ah_e = 2.22 \frac{k_{vi}}{D_s^2} \left(\frac{\rho_{vi} \Delta V D_s}{\mu_{vi}} \right)^{0.6} \frac{W_l}{\rho_l A_c V_l} \tag{21}$$

which gives the effective evaporation heat transfer coefficient in terms of the mechanics of the evaporation process. By expressing the liquid flow rate as the total less the vapor flow and the liquid velocity as the vapor velocity less the slip velocity, equation (21) is reduced to the form:

$$a h_e = 2.22 \frac{k_{vi}}{D_s^2} \left(\frac{\rho_{vi} \Delta V D_s}{\mu_{vi}} \right)^{0.6} \frac{\rho_v}{\rho_\ell} \left(\frac{\frac{G}{\rho_v V_v} - 1}{1 - \frac{\Delta V}{V_v}} \right) \tag{22}$$

Since vapor velocity can be estimated in the quality range of interest by the equation:

$$V_v = \frac{W_v}{\rho_v A_c} = \frac{4 \frac{Q}{A} L}{\rho_v D_w (H_v - H_\ell)} \tag{23}$$

the only variables left in equation (19) are drop size and slip velocity. By writing a force balance on a single drop of diameter D_s, the slip velocity is obtained in the form:

$$(V_v - \Delta V) \frac{dV_s}{dL} = \frac{3}{4} \frac{C_D}{D_s} \frac{\rho_v}{\rho_\ell} (\Delta V)^2 - g \tag{24}$$

which upon reduction yields:

$$\Delta V = \frac{-\frac{1}{2} \frac{dV_s}{dL} \pm \sqrt{\frac{1}{4} \left(\frac{dV_s}{dL} \right)^2 + \frac{3}{4} \frac{C_D}{D_s} \frac{\rho_v}{\rho_\ell} \left(V_v \frac{dV_s}{dL} + g \right)}}{\frac{3}{4} \frac{C_D}{D_s} \frac{\rho_v}{\rho_\ell}} \tag{25}$$

Although equation (25) is not in closed form because of the presence of the derivative, $\frac{dV_s}{dL}$, a first estimate of ΔV may be made by assuming that $\frac{d(\Delta V)}{dL}$ is small so that $\frac{dV_s}{dL} = \frac{dV_v}{dL}$. Figure 19 shows the results of such an assumption for two different sized drops exposed to the conditions of run 53. The variation of drop diameter

with length was estimated, assuming that $(Q_e)_{drop} = m_{drop}\left(\frac{Q_e}{m_\ell}\right)_L$, by the equation:

$$\frac{D_L}{D_o} = e^{-\int_{L_o}^{L} \frac{1}{3\omega_\ell (H_v - H_\ell)} \frac{dQ_e}{dL} dL} \tag{26}$$

For the small drop, D_o = .1mm, it was found the assumption was adequate while for the larger drop, D_o = 1mm, it was found that a better assumption was $\frac{dV_s}{dL} = .63 \frac{dV_v}{dL}$. Since the solution of equation (25) implies an initial slip velocity, equation (24) was solved by finite difference techniques to determine the effect of greater values of ΔV at L_o. The dashed lines of Figure 19 show the results of these calculations and indicate that the use of equation (25) to calculate slip velocity is a valid procedure.

Mean Effective Drop Size

By the simultaneous solution of equations (22) and (25) it is now possible to calculate a mean effective drop size at various lengths for any of the experimental runs. Figure 20 shows the results of these calculations for runs covering the entire flow rate, heat flux range of the experimental program. In solving equation (25) a drag coefficient of .5 and linear interpolation of $\frac{dV_s}{dL}$ with drop size between $\frac{dV_s}{dL} = \frac{dV_v}{dL}$ at D_s = .1mm and $\frac{dV_s}{dL} = .6 \frac{dV_v}{dL}$ at 1mm, were found to be adequate for all cases. The drop diameters shown in Figure 20 are all less than 1mm as would be expected from the visual

studies. In the calculated drop sizes for runs 3 and 53, the rate of decrease of drop size with increasing quality is seen to decrease at higher quality corresponding to the end of drop break-up. At the lowest quality value shown for runs 31 to 51, the calculated drop size decreases because of the ah_e increase created by breakdown of the two step theory. As would be expected from the mechanics of the break-up process, higher heat fluxes, with the attendant increase in vapor acceleration, give smaller drop sizes at the same quality while higher flow rates which need greater tube lengths to produce the same quality, also produce smaller drop sizes.

In Figure 21 a correlation of the drop size data is shown for the range of the two step theory in which break-up of drops is present. Since no check of the correlation to determine the effect of fluid properties or tube diameter is possible within the scope of this work, it is presented without assurance that it is applicable over a broader range of variables than those encompassed herein.

Because of the sensitivity of equation (16) to not only vapor temperature but also $\frac{dT_v}{dL}$, the use of the drop size correlation to predict wall temperatures and overall heat transfer coefficients for film boiling is not possible. However, in spite of the failure of the theory to produce a useable heat transfer correlation, much has been learned about the mechanics of the film boiling process through the success of the drop size calculations. Most important, it has been confirmed that a two step process will work. Therefore,

if the local vapor temperature is known, the wall temperature and heat transfer coefficient may be calculated simply by use of equations (17) and (13) respectively, as long as the basic assumption of inlet conditions, uniform heat flux and dispersed flow are met. As a guide to determine the minimum quality for which the dispersed flow condition is met, Figure 22 shows the limits of the theory found for the experimental range covered in this program. Although the vapor temperature will be unknown in most cases, an upper bound on the heat transfer coefficient will be obtained from the equations by assuming that the vapor is at saturation temperature. Since this implies equilibrium between the phases, the corresponding upper bound of quality is given by the equation:

$$X = \frac{L}{L_{sat}} \tag{27}$$

In Figure 23 the actual quality for typical experimental runs, calculated by dividing equation (15) by the total flow rate, is compared with the equilibrium condition of equation (27). The departure of the data from the equilibrium condition is related to local vapor temperature through the equation:

$$H_v = H_l + 4 \frac{Q}{A} \frac{L}{G D_w X} \tag{28}$$

Therefore, if it is desired to make an estimate of the film boiling heat transfer coefficient which is better than the upper bound presented above, the value of vapor temperature may be obtained using Figure 23 in conjunction with equation (28). In making this suggestion it seems well to point out that the displacement of the data from the equilibrium condition is dependent upon the mechanics of the evaporation process. Consequently, it would be expected that increased heat flux and increased mass flow rate would move the process toward the equilibrium condition and that decreases of these variables would move it away. In addition, variation of fluid properties would undoubtedly have a strong effect while tube diameter effects might well be accounted for by using volume heat flux, $\frac{1}{D_w}\frac{Q}{A}$, in correlating heat flux effects.

Conclusion

In conclusion, the results obtained from the analysis are summarized as follows:

1. For film boiling of saturated liquid flowing upward through a uniformly heated vertical tube, there are two basic flow regimes: near the inlet the flow is annular with liquid in the core and vapor in the annulus; at higher vapor fractions the core is broken up to give a dispersed flow regime in which droplets and filaments are carried along in a vapor matrix.

2. In the case of nitrogen, the thickness of the vapor annulus grows very rapidly so the theory derived by Dougall (7), for film boiling at small vapor fractions, does not agree with the experimental results obtained with nitrogen.

3. In most cases the break-up of annular flow is gradual and tube wall temperature reaches a simple maximum in the vicinity of the transition but at mass velocities greater than about 180,000 lbm/hr-ft^2, with high heat fluxes, there is a depression of wall temperature following the maximum which indicates that a critical Weber number may be involved at which the break-up begins suddenly.

4. Once transition has proceeded to the degree that drops are relatively uniformly dispersed, the heat transfer may be considered to be a two step process in which 1) all of the heat from the wall is transferred to the vapor and 2) heat is transferred from the vapor to the liquid.

a. The heat transfer coefficient between the wall and the vapor is given approximately by the equation:

$$\frac{h_1 D_w}{k_v} = .023\left[\frac{\rho_v D_w}{\mu_v}\left(\frac{q_v + q_l}{A_c}\right)\right]^{0.8} Pr_v^{0.4} \qquad (11)$$

b. Evaporation rate of the liquid is controlled by drop size, vapor velocity and acceleration, and vapor temperature.

c. Because the evaporation heat transfer coefficient is not large compared to the wall-to-vapor coefficient, a significant amount of vapor superheat is present and it is impossible to obtain

a simple expression for the overall heat transfer coefficient.

d. Use of Figures 22 and 23 together with equations (13) and (17) provides a method by which both an upper bound and an approximation for the actual heat transfer coefficient can be obtained in the region of validity of the theory.

NOMENCLATURE

a	Surface area of drops per unit volume of liquid-vapor mixture
A_c	Cross sectional area for fluid flow through the test section
C_D	Drag coefficient
C_p	Specific heat
D_d	Drop diameter
D_s	Equivalent mean drop diameter for the evaporation process
D_w	Inside diameter of the test section
E	Voltage drop across the test section
G	Mass velocity,
g	Gravitational acceleration
h	Overall heat transfer coefficient at any location along the test section
h_l	Local heat transfer coefficient between the wall and the vapor
h_e	Evaporation heat transfer coefficient
h_{fg}	Latent heat
H	Enthalpy
I	Electric current passing through the walls of the test section
Jg_o	Mechanical equivalent of heat conversion factor
k	Thermal conductivity
L	Distance from the start of the test section
L_o	Total length of the test section
L_{sat}	Length to complete evaporation in an equilibrium process
m	Mass
N	Concentration of drops of a given size, $\frac{dn}{dD_d}$

NOMENCLATURE (Continued)

n	Number of drops per unit volume of liquid-vapor mixture
P_i	Pressure at the test section inlet
ΔP	Pressure drop across the test section
Pr	Prandtl number, $\frac{c_p \mu}{k}$
$\frac{Q}{A}$	Heat flux from the walls of the test section
Q_{loss}	Total thermal loss from the outer surface of the test section
Q_e	Heat going into evaporation
$\frac{Q_e}{\mathcal{V}}$	Heat going into evaporation per unit volume of liquid-vapor mixture
q_l	Average volume flow rate of liquid at any location along the test section
q_v	Average volume flow rate of vapor at any location along the test section
R	Electrical resistance
r	Electrical resistivity
T_f	Average temperature of the vapor boundary layer at the wall, $\frac{1}{2}(T_w+T_v)$
T_i	Average temperature of the vapor at the evaporation interface on a drop of liquid $\frac{1}{2}(T_v+T_s)$
T_v	Vapor temperature
T_w	Wall temperature (on the inside surface of the test section)
T_{wo}	Temperature on the outside surface of the test section
V_d	Drop velocity

NOMENCLATURE (Continued)

V	Liquid drop velocity
ΔV	Slip velocity, $V_v - V_e$
ω_v	Mass flow rate of vapor
ω_l	Mass flow rate of liquid
ω_t	Total mass flow rate
X	Quality, $\frac{\omega_v}{\omega_t}$
δ_{ss}	Wall thickness of the 304 stainless steel test section
μ	Viscosity
σ	Surface tension
ρ	Density

Subscripts

b	Quantities evaluated at bulk temperature (see eqn. 7)
buss	Refers to copper buss bars connecting the test section to the power cables
eq	Quantities evaluated assuming an equilibrium process
f	Quantities evaluated at film temperature, T_f
i	Quantities evaluated at interface temperature, T_i
L	Quantities evaluated at a length L
l	Quantities evaluated for saturated liquid
sat	Saturation
ss	Quantities refering to stainless steel test section
v	Quantities evaluated for vapor at T_v or at some other temperature if specified by a second subscript.

BIBLIOGRAPHY

1. Bromley, L.A.
"Heat Transfer in Film Boiling"
Chemical Engineering Progress, Vol. 46, 1950, p. 221.

2. McFadden, P.W., and Grosh, R.J.
"High-Flux Heat Transfer Studies: An Analytical Investigation of Laminar Film Boiling"
AEC Research and Development Report, ANL-6060, 1959.

3. Koh, J.C.Y.
"Analysis of Film Boiling on Vertical Surfaces"
ASME Paper No. 61-SA-31.

4. Carter, J.C.
"The Effect of Film Boiling"
AEC Research and Development Report, ANL-6291, 1961.

5. Kruger, R.A.
"Film Boiling on the Inside of Horizontal Tubes in Forced Convection"
M.I.T. Ph.D. Thesis, June, 1961.

6. Doyle, E.F.
"Effect of Subcooling on Film Boiling in a Horizontal Tube"
S.M. Thesis, M.I.T., June, 1962.

7. Dougall, R.S.
"Film Boiling on the Inside of Vertical Tubes with Upward Flow of the Fluid at Low Qualities"
M.I.T., Department of Mechanical Engineering, EPL Report No. 9079-26.

8. Hendricks, R.C., Graham, R.W., Hsu, Y.Y., and Friedman, R.
"Experimental Heat Transfer and Pressure Drop of Liquid Hydrogen Through a Heated Tube"
NASA TN D-765, May, 1961.

9. Lewis, J.P., Goodykoontz, J.H., and Kline, J.F.
"Boiling Heat Transfer to Liquid Hydrogen and Nitrogen in Forced Flow"
NASA TN D-1314, Sept., 1962.

10. Parker, J.D., and Grosh, R.J.
"Heat Transfer to a Mist Flow"
AEC Research and Development Report, ANL-6291, 1961.

BIBLIOGRAPHY (Continued)

11. Lavin, J.G. and Young, E.H.
"Heat Transfer to Evaporating Refrigerants in Two-Phase Flow"
Preprint 21e AIChE Fifty Second Annual Meeting, Memphis, Tenn., February 1964.

12. Polomik, E.E., Levy, S., and Sawochka, S.G.
"Film Boiling of Steam-Water Mixtures in Annular Flow at 800, 1100, and 1400 Psi"
ASME Paper No. 62-WA-136.

13. Scott, R.B.
Cryogenic Engineering D. Van Nostrand Co., Inc., Princeton, N.J., 1959.

14. Chelton, D.B. and Mann, D.B.
"Cryogenic Data Book"
U.S. Air Force, WADC Technical Report 59-8, 1959.

15. Strobridge, T.R.
"The Thermodynamic Properties of Nitrogen from 64 to 300^{o}K Between 0.1 and 200 Atmospheres" NBS TN 129, January 1962.

16. Handbook of Chemistry and Physics
Chemical Rubber Publishing Co.,
Forty-Third Edition, 1961-1962.

17. McAdams, W.H.
Heat Transmission
McGrall-Hill Book Co., Inc.
New York, 1954.

18. Humble, L.V., Lowdermilk, W.H., and Desmon, L.G.
"Measurements of Average Heat-Transfer and Friction Coefficients for Subsonic Flow of Air in Smooth Tubes at High Surface and Fluid Temperatures"
NACA Report 1020, 1951.

APPENDIX A

DISCUSSION OF ERRORS

The experimental errors were of three types: those due to instrumentation accuracy and sensitivity, those caused by system losses and those caused by system instabilities. It is useful to discuss separately errors in the four measured items: flow, heat flux, pressure and temperature.

The errors in flow measurement were due to lack of sensivitiy of the rotameter and to system instabilities. The rotameter was calibrated for ± 1% of full scale accuracy which gives an absolute error of ± 1.2 lbm/hr. Therefore the reading accuracy of flow rate varies from ± 3.1% at the lowest flow rate to ± 1% at the highest flow rate. Because the system is a once through boiler there are inherent instabilities. For a flow of the runs flow oscillations occurred which amounted to as much as ± 2 lbm/hr but generally the fluctuations were only about ± 1 lbm/hr. In no case were the temperature and pressure flow correction factors large enough to make errors in the corresponding temperature and pressure measurements significant.

Heat conduction losses out of the inlet buss bar and power measurement errors were the two sources of heat flux error. The conduction loss was calculated for each run and was found always to be less than 1% of the power input. Since it is really an end effect rather than a heat flux loss, it can be considered to be a length error of less than 1% of the total length or less than

½ inch. In no case does wall temperature vary significantly in a ½ inch interval. Therefore the conduction loss was negligible and no correction was made to account for it. Also, because of the lack of large axial temperature gradients in the wall, non-uniformities in heat flux due to axial heat conduction were found to be negligible. The measurement error for input power was ± ½% of full scale for both the ammeter and voltmeter. This gives a maximum heat flux error at the lowest power inputs of ± 2.6% and at the highest power inputs of about ± 1%.

The inlet pressure measurement was sufficiently accurate to give an overall accuracy after correction for barometric pressure of ± ½%. The measurement of test section pressure drop had an absolute accuracy of about ± .02 psi. Instabilities in the flow system account for most of the pressure error. Since the test section pressure drop was relatively small these fluctuations caused errors of up to 5% in that reading.

The measurement of temperature was found to be the largest source of errors. Although the thermocouples were calibrated over the entire range of operating temperatures, it was very difficult to install them in the system so that lead wire conduction would not produce an erroneous reading. Because of the necessity of electrically insulating the thermocouples from the test section it was necessary also to, at least slightly, thermally insulate the junction from the tube. If a sufficient length of lead had been firmly cemented to

the tube, and if conduction and radiation from the free surface of the junction had been completely eliminated , the thermocouple should have read the surface temperature of the tube to within ± 6°F at the maximum wall temperature and to within ± 3°F at the minimum wall temperature. However, this junction insulation was not achieved and, at the highest wall temperatures there appeared to be an error of about -35°F or about -3.5% in wall superheat. More seriously, at negative temperatures (i.e. low heat fluxes), conduction from the surroundings through the lead wires produced errors of up to +15°F or about 7.5% in wall superheat. Because the exact size of these errors is very difficult to measure in this particular system and because the error encountered over most of the range of data is less than 3% of the wall superheat, no correction of the temperature measurements was attempted. The Brown self-balancing potentiometer which was used to record the thermocouple emf's has an absolute accuracy of ± .045 mv. This gives an error of less than 1.5% of the wall superheat in all cases but gives an error of ± 5°F for the test section inlet temperature at liquid nitrogen saturation temperature. Somewhat larger errors in the readings of this thermocouple were encountered during operation. This deviation was unaccountable but the stability of the thermocouple was sufficiently good to indicate when stable inlet conditions were attained.

Another source of temperature error lies in the conduction loss in the tube wall. Since the temperature which is desired in the

inside surface temperature and the thermocouple is on the external surface, the temperature difference between the surfaces constitutes a temperature error. For simplification, assume that the wall is a plane surface with uniform heat generation and one side perfectly insulated. Since the wall thickness is small, and since the wall is hotter on the external surface so that the heat generation actually decreases from the inside to the outside, these assumptions will over estimate the error. The solution to the conduction equation then gives the equation:

$$T_w - T_{w_o} = \frac{Q}{A} \frac{\delta_{ss}}{2 k_{ss}} \tag{29}$$

At even the highest heat flux of the experimental program this solution gives no more than a $5^{\circ}F$ error and that acts in a direction to compensate for the measurement error discussed above.

APPENDIX B

VARIATION OF THE ELECTRICAL RESISTIVITY OF THE STAINLESS STEEL 304 TEST SECTION

Since many investigators use the I^2R technique of measuring power input for electrically heated systems, it seems pertinent to comment here on an anomaly encountered in trying to use this method for a check on the heat flux measurements of this program. In order to have an accurate value of test section resistance it was decided that it would be best to measure the resistance directly rather than use a handbook value, which would not account for the effects of variation of composition and machining.

A series circuit consisting of a 2 volt wet cell battery, a load resistor, a Leeds and Northrop .001 ohm standard resistor and the test section, was set up for the measurements. The load resistor was set to give a current of about 9 amperes so that the voltage drop across the standard resistor could be read on one channel of the Brown recorder. The remaining 15 channels were used to record tube wall temperature as usual. A Leeds and Northrop precision potentiometer was used to read the voltage drop between the end flanges of the test section.

Three different types of tests were conducted; room temperature tests, hot tests during transient cool-down and cold tests during transient warm-up. The tube was heated for the hot tests with the test section power supply. Since a transformer is used in the supply it was necessary to open the power circuit before measurements could be

made. The test section was cooled to liquid nitrogen temperature for the cold tests by running the liquid nitrogen through the apparatus with the power supply disconnected. For both the hot and cold tests the test section with its asbestos insulation was cooled or warmed to room temperature by natural convection. As the transient condition continued, the precision potentiometer was balanced to read the test section voltage at the same instant the recorder was reading standard resistor voltage. The average temperature at that same time was obtained by drawing a best fit curve through the temperature points on the recorder chart. The measurement system produced a scatter, for each transient run, of less than ½% from the best fit line on a resistivity-temperature plot.

The results of the tests are shown in Figure 25 numbered in the order in which the runs were made. Between numbers 5 and 6 the tube was heated to about 250°F but otherwise each run followed the preceding one with no temperature changes in between. The dashed lines in Figure 25 show the limits of resistivity variation obtained from the current and voltage measurements made for the film boiling experimental data. Under normal operation the tube was never cooled to liquid nitrogen temperature so these limits are less than the data of the cold runs made for the resistivity measurements.

Obviously there is some change in the resistivity of the 304 stainless steel tube caused by lowering its temperature to about -320°F. It may be a martensitic phase change but the return of the resistivity

to lower values after a period at room temperature would not seem to support this argument. Whatever the cause, the fact that exposure to cryogenic temperature caused the resistivity of 304 stainless steel to change, is sufficient grounds to warrant complete power sensing instrumentation in such applications.

TABLE I

THERMOCOUPLE LOCATIONS

Symbol for Location	Distance from Start of Heated Section (inches)
L_1	2.4
L_2	5.5
L_3	8.5
L_4	11.5
L_5	14.7
L_6	17.6
L_7	20.4
L_8	23.5
L_9	26.5
L_{10}	29.5
L_{11}	32.4
L_{12}	35.4
L_{13}	38.4
L_{14}	41.4
L_{15}	44.5

TABLE II

DATA FOR THE QUANTITATIVE TEST SECTION

RUN	1	2	3
G - lbm/hr-ft^2	69900	69700	70200
I - amps	136.5	137	153
E - volts	7.03	7.06	7.95
(q/A) - Btu/hr-ft^2	9720	9800	12300
P_i - psia	17.00	17.04	17.54
ΔP - psi	.58	.60	.75
T_s - ^oR	141	142	142

Location	T_w-T_s (^oF)	h (Btu/hr-ft^2-^oF)	T_w-T_s (^oF)	h (Btu/hr-ft^2-^oF)	T_w-T_s (^oF)	h (Btu/hr-ft^2-^oF)
L_1	527	18.2	505	18.9	655	18.9
L_2	578	17.0	557	17.5	704	17.9
L_3	596	16.6	579	17.0	702	18.1
L_4	590	16.8	579	17.1	681	18.4
L_5	591	16.7	586	16.9	679	18.4
L_6	584	16.9	582	17.0	664	18.7
L_7	576	17.0	577	17.2	653	18.9
L_8	568	17.1	572	17.3	641	19.2
L_9	564	17.3	572	17.2	638	19.1
L_{10}	555	17.5	558	17.6	619	19.7
L_{11}	548	17.7	556	17.5	614	19.8
L_{12}	540	17.9	546	17.8	602	20.0
L_{13}	546	17.6	546	17.8	602	20.0
L_{14}	526	18.2	536	18.1	591	21.4
L_{15}	525	18.1	534	18.1	592	22.3

TABLE II (Continued)

RUN	4	5	6
G - lbm/hr-ft^2	71000	71600	74500
I - amps	121	106	106
E - volts	6.04	4.95	4.95
(q/A) - Btu/hr-ft^2	7380	5310	3720
p_i - psia	16.96	16.98	17.41
ΔP - psi	.66	.41	.35
T_s - ^oR	141	141	142

Location	T_w-T_s (^oF)	h (Btu/hr-ft^2-^oF)	T_w-T_s (^oF)	h (Btu/hr-ft^2-^oF)	T_w-T_s (^oF)	h (Btu/hr-ft^2-^oF)
L_1	393	17.8	295	17.2	224	16.0
L_2	433	16.5	313	16.3	225	16.0
L_3	462	15.7	336	15.4	237	15.2
L_4	477	15.4	351	14.9	259	14.0
L_5	492	15.1	359	14.7	270	13.5
L_6	498	14.9	373	14.3	286	12.9
L_7	501	14.8	383	13.9	296	12.5
L_8	502	14.8	393	13.6	310	12.0
L_9	504	14.8	399	13.4	313	11.9
L_{10}	501	14.8	403	13.4	328	11.4
L_{11}	500	14.9	406	13.3	329	11.4
L_{12}	495	15.0	409	13.3	339	11.1
L_{13}	494	15.0	413	13.1	338	11.2
L_{14}	486	15.2	413	13.1	340	11.2
L_{15}	485	15.3	413	13.1	343	11.2

TABLE II (Continued)

RUN	7	8	9
G - lbm/hr-ft^2	76100	119900	114700
I - amps	92	116	133
E - volts	4.0	5.04	5.97
(q/A) - Btu/hr-ft^2	3720	5910	8030
P_i - psia	17.41	17.41	16.70
ΔP - psi	.35	.56	.70
T_s - ^oR	142	142	141

Location	T_w-T_s (^oF)	h (Btu/hr-ft^2-^oF)	T_w-T_s (^oF)	h (Btu/hr-ft^2-^oF)	T_w-T_s (^oF)	h (Btu/hr-ft^2-^oF)
L_1	202	17.6	221	25.7	285	27.2
L_2	201	17.8	227	25.2	290	26.8
L_3	213	16.8	236	24.4	308	25.5
L_4	237	15.2	255	22.8	332	24.0
L_5	249	14.7	267	21.9	347	23.2
L_6	266	13.9	280	21.0	357	22.6
L_7	277	13.4	287	20.6	363	22.4
L_8	292	12.8	296	20.1	368	22.0
L_9	298	12.6	297	20.1	369	22.1
L_{10}	314	12.0	307	19.6	373	21.8
L_{11}	316	12.0	306	19.7	373	21.8
L_{12}	327	11.7	314	19.2	375	21.8
L_{13}	329	11.6	312	19.3	372	21.9
L_{14}	334	11.5	312	19.3	369	22.1
L_{15}	339	11.7	312	19.3	368	22.2

TABLE II (Continued)

RUN	10	11	12
G - lbm/hr-ft^2	112900	111000	110300
I - amps	151	168	184
E - volts	7.05	7.98	8.96
(q/A) - Btu/hr-ft^2	10800	13600	16800
P_i - psia	17.82	17.97	18.20
ΔP - psi	.87	1.06	1.32
T_s - ^oR	142	142	143

Location	T_w-T_s (^oF)	h (Btu/hr-ft^2-^oF)	T_w-T_s (^oF)	h (Btu/hr-ft^2-^oF)	T_w-T_s (^oF)	h (Btu/hr-ft^2-^oF)
L_1	377	27.9	490	27.7	593	28.9
L_2	383	27.6	500	27.4	601	28.7
L_3	407	26.2	516	26.6	602	28.6
L_4	420	25.6	513	26.8	586	29.3
L_5	430	25.2	516	26.6	582	29.4
I_6	433	25.0	510	26.9	572	29.7
L_7	435	24.9	507	27.0	563	30.0
L_8	437	24.9	504	27.2	555	30.4
L_9	437	24.8	500	27.4	549	30.6
L_{10}	434	25.0	490	27.8	533	31.2
L_{11}	432	25.1	486	28.0	526	31.5
L_{12}	428	25.3	477	28.4	512	32.2
L_{13}	424	25.5	472	28.6	507	32.4
L_{14}	416	25.9	458	29.3	491	33.2
L_{15}	412	26.1	453	29.4	486	33.3

TABLE II (Continued)

RUN	13	14	15
G - lbm/hr-ft^2	110700	155200	155200
I - amps	184	196	213
E - volts	9.0	9.02	9.95
(q/A) - Btu/hr-ft^2	16900	17100	21600
P_i - psia	18.52	18.87	19.26
ΔP - psi	1.26	1.57	2.16
T_s - ^oR	143	143	144

Location	T_w-T_s (^oF)	h (Btu/hr-ft^2-^oF)	T_w-T_s (^oF)	h (Btu/hr-ft^2-^oF)	T_w-T_s (^oF)	h (Btu/hr-ft^2-^oF)
L_1	668	26.6	515	33.8	590	38.1
L_2	655	27.0	494	35.0	556	39.8
L_3	631	27.8	498	34.8	554	40.0
L_4	605	28.7	494	35.2	544	40.5
L_5	597	28.7	495	35.0	544	40.4
L_6	583	29.2	491	35.2	537	40.8
L_7	573	29.6	489	35.4	533	41.0
L_8	564	30.0	486	35.5	527	41.3
L_9	556	30.2	479	36.0	519	41.8
L_{10}	539	31.0	469	36.5	502	42.7
L_{11}	530	31.2	461	36.9	491	43.4
L_{12}	516	31.8	452	37.4	477	44.4
L_{13}	510	32.0	442	38.0	468	45.0
L_{14}	493	33.0	426	39.2	450	46.5
L_{15}	489	33.2	418	39.7	442	47.0

TABLE II (Continued)

RUN	16	17	18
G - lbm/hr-ft^2	154000	157200	204000
I - amps	226.5	180.5	229.5
E - volts	11.0	8.03	10.45
(q/A) - Btu/hr-ft^2	25400	14700	24400
P_i - psia	19.65	18.67	20.42
ΔP - psi	2.34	1.35	2.53
T_s - ^oR	144	143	145

Location	T_w-T_s (^oF)	h (Btu/hr-ft^2-^oF)	T_w-T_s (^oF)	h (Btu/hr-ft^2-^oF)	T_w-T_s (^oF)	h (Btu/hr-ft^2-^oF)
L_1	710	38.3	394	36.7	444	54.7
L_2	658	40.4	411	35.6	530	47.9
L_3	638	41.1	414	35.5	460	53.4
L_4	615	42.3	421	35.0	458	53.4
L_5	612	42.3	427	34.6	468	52.5
L_6	598	43.1	429	34.6	470	52.5
L_7	588	43.5	428	34.7	472	52.1
L_8	577	44.2	429	34.5	472	52.0
L_9	565	44.7	424	34.9	466	52.6
L_{10}	542	46.1	422	35.0	458	53.5
L_{11}	528	47.0	416	35.3	450	54.1
L_{12}	510	48.4	414	35.4	440	55.0
L_{13}	500	49.0	404	36.2	429	56.2
L_{14}	480	50.5	393	37.0	412	58.0
L_{15}	475	53.8	387	37.4	403	59.0

TABLE II (Continued)

RUN	19	20	21
G - lbm/hr-ft^2	204000	205000	207000
I - amps	241	215	195
E - volts	11.1	9.3	8.45
(q/A) - Btu/hr-ft^2	26300	20400	16800
P_i - psia	20.73	19.95	19.63
ΔP - psi	2.86	2.14	1.86
T_s - ^oR	145	144	144

Location	T_w-T_s (^oF)	h (Btu/hr-ft^2-^oF)	T_w-T_s (^oF)	h (Btu/hr-ft^2-^oF)	T_w-T_s (^oF)	h (Btu/hr-ft^2-^oF)
L_1	486	54.0	344	57.5	344	48.0
L_2	565	48.6	425	49.0	411	41.7
L_3	494	53.5	392	51.9	367	44.8
L_4	491	54.0	385	52.9	369	45.5
L_5	502	53.0	395	51.8	378	44.4
L_6	503	52.9	404	50.8	383	44.0
L_7	504	52.7	407	50.5	386	43.8
L_8	503	52.5	412	49.9	389	43.6
L_9	495	53.3	410	50.3	386	43.9
L_{10}	482	54.5	410	50.0	387	43.6
L_{11}	474	55.1	406	50.5	382	44.1
L_{12}	461	56.2	403	50.8	382	44.1
L_{13}	450	57.4	393	51.9	371	45.3
L_{14}	430	59.5	380	53.4	361	46.3
L_{15}	422	60.5	375	53.9	356	46.7

TABLE II (Continued)

RUN	22	23	24
G - lbm/hr-ft^2	211000	215000	216000
I - amps	178	160	142.5
E - volts	7.55	6.55	5.62
(q/A) - Btu/hr-ft^2	13700	10700	8130
P_i - psia	19.34	19.03	18.78
ΔP - psi	1.55	1.34	1.16
T_s - ^oR	144	143	143

Location	T_w-T_s (^oF)	h (Btu/hr-ft^2-^oF)	T_w-T_s (^oF)	h (Btu/hr-ft^2-^oF)	T_w-T_s (^oF)	h (Btu/hr-ft^2-^oF)
L_1	286	46.5	231	45.1	187	42.0
L_2	335	40.9	252	41.9	191	41.8
L_3	334	41.0	272	39.1	208	38.6
L_4	324	42.0	264	40.2	214	37.6
L_5	332	41.0	267	40.0	211	38.1
L_6	340	40.2	279	38.4	223	36.2
L_7	343	40.0	282	38.2	226	36.0
L_8	348	39.5	291	37.0	236	34.6
L_9	346	39.8	289	37.3	234	35.0
L_{10}	349	39.4	300	36.0	249	33.0
L_{11}	349	39.4	293	36.9	243	33.9
L_{12}	349	39.4	304	35.6	259	35.9
L_{13}	341	40.3	295	36.6	248	33.3
L_{14}	335	40.9	295	36.6	251	32.9
L_{15}	332	41.0	293	36.9	251	33.0

TABLE II (Continued)

RUN	25	26	27
G - lbm/hr-ft^2	69700	69600	69900
I - amps	153	144	139
E - volts	7.85	7.27	6.93
(q/A) - Btu/hr-ft^2	12200	10600	9760
P_i - psia	17.28	17.19	17.15
ΔP - psi	.77	.72	.66
T_s - ^oR	142	142	142

Location	T_w-T_s (^oF)	h (Btu/hr-ft^2-^oF)	T_w-T_s (^oF)	h (Btu/hr-ft^2-^oF)	T_w-T_s (^oF)	h (Btu/hr-ft^2-^oF)
L_1	642	19.2	547	19.0	506	18.8
L_2	682	18.3	605	17.8	564	17.3
L_3	677	18.5	614	17.5	577	17.0
L_4	661	18.8	608	17.7	577	17.1
L_5	659	18.8	609	17.7	582	16.9
L_6	644	19.2	600	17.9	577	17.1
L_7	635	19.4	595	18.0	574	17.2
L_8	626	19.5	590	18.1	571	17.3
L_9	623	19.5	588	18.0	570	17.2
L_{10}	604	20.1	573	18.4	557	17.5
L_{11}	601	20.1	571	18.4	556	17.5
L_{12}	586	20.5	557	18.8	544	17.8
L_{13}	590	20.3	559	18.7	547	17.6
L_{14}	577	21.7	547	19.0	535	18.0
L_{15}	578	22.6	547	19.0	534	18.0

TABLE II (Continued)

RUN	28	29	30
G - lbm/hr-ft^2	70000	71000	72000
I - amps	132	124	116
E - volts	6.45	5.87	5.40
(q/A) - Btu/hr-ft^2	8600	7320	6320
P_i - psia	17.04	17.04	16.98
ΔP - psi	.58	.48	.50
T_s - ^oR	142	142	141

Location	T_w-T_s (^oF)	h (Btu/hr-ft^2-^oF)	T_w-T_s (^oF)	h (Btu/hr-ft^2-^oF)	T_w-T_s (^oF)	h (Btu/hr-ft^2-^oF)
L_1	445	18.6	374	18.7	320	18.8
L_2	493	17.3	415	17.2	353	17.3
L_3	515	16.7	442	16.4	381	16.4
L_4	522	16.6	457	16.0	400	15.7
L_5	533	16.3	472	15.6	418	15.1
L_6	533	16.3	477	15.5	428	14.9
L_7	534	16.3	482	15.3	435	14.6
L_8	534	16.3	484	15.3	441	14.5
L_9	536	16.2	487	15.2	447	14.3
L_{10}	527	16.4	484	15.3	447	14.3
L_{11}	526	16.4	484	15.3	449	14.3
L_{12}	517	16.7	480	15.4	448	14.3
L_{13}	519	16.6	481	15.4	449	14.3
L_{14}	509	16.9	474	15.6	445	14.4
L_{15}	508	16.9	474	15.6	445	14.4

TABLE II (Continued)

RUN	31	32	33
G - lbm/hr-ft^2	73400	73600	75000
I - amps	108	101	93
E - volts	4.85	4.45	3.97
(q/A) - Btu/hr-ft^2	5300	4550	3740
P_i - psia	16.88	17.03	16.95
ΔP - psi	.43	.37	.37
T_s - ^oR	141	142	141

Location	T_w-T_s (^oF)	h (Btu/hr-ft^2-^oF)	T_w-T_s (^oF)	h (Btu/hr-ft^2-^oF)	T_w-T_s (^oF)	h (Btu/hr-ft^2-^oF)
L_1	271	18.5	235	18.4	193	18.5
L_2	292	17.4	242	18.0	193	18.5
L_3	315	16.2	262	16.8	208	17.4
L_4	337	15.3	284	15.6	228	16.0
L_5	352	14.9	302	14.9	241	15.2
L_6	366	14.5	319	14.2	261	14.1
L_7	375	14.2	329	13.8	270	13.7
L_8	385	13.9	342	13.4	284	13.2
L_9	390	13.8	347	13.3	290	13.0
L_{10}	397	13.6	355	13.0	307	12.4
L_{11}	399	13.6	358	13.0	308	12.4
L_{12}	403	13.4	366	12.8	323	11.9
L_{13}	404	13.4	367	12.8	319	12.1
L_{14}	404	13.4	369	12.8	327	11.8
L_{15}	405	13.4	371	12.8	330	11.7

TABLE II (Continued)

RUN	34	35	36
G - lbm/hr-ft^2	119800	117700	114500
I - amps	112	118	133
E - volts	4.71	5.09	5.98
(q/A) - Btu/hr-ft^2	5340	6060	8060
P_i - psia	17.55	17.51	17.63
ΔP - psi	.60	.60	.70
T_s - ^oR	142	142	142

Location	T_w-T_s (^oF)	h (Btu/hr-ft^2-^oF)	T_w-T_s (^oF)	h (Btu/hr-ft^2-^oF)	T_w-T_s (^oF)	h (Btu/hr-ft^2-^oF)
L_1	204	25.1	235	24.9	308	25.4
L_2	212	24.3	237	24.8	314	25.0
L_3	218	23.8	250	23.6	333	23.8
L_4	233	22.4	267	22.3	349	22.9
L_5	245	21.5	280	21.5	358	22.5
L_6	260	20.4	294	20.6	365	22.2
L_7	265	20.1	299	20.3	369	22.0
L_8	275	19.5	308	19.8	374	21.7
L_9	276	19.4	309	19.8	374	21.7
L_{10}	287	18.7	319	19.3	377	21.6
L_{11}	285	18.9	317	19.4	375	21.7
L_{12}	297	18.2	326	18.9	377	21.6
L_{13}	291	18.6	321	19.2	374	21.7
L_{14}	294	18.4	322	19.2	370	21.9
L_{15}	295	18.4	322	19.2	368	22.0

TABLE II (Continued)

RUN	37	38	39
G - lbm/hr-ft^2	112700	110100	109600
I - amps	151	168	183
E - volts	6.95	8.05	9.02
(q/A) - Btu/hr-ft^2	10600	13700	16800
P_i - psia	17.72	17.92	18.13
ΔP - psi	.85	1.01	1.28
T_s - ^oR	142	142	143

Location	T_w-T_s (^oF)	h (Btu/hr-ft^2-^oF)	T_w-T_s (^oF)	h (Btu/hr-ft^2-^oF)	T_w-T_s (^oF)	h (Btu/hr-ft^2-^oF)
L_1	391	26.7	555	25.2	686	25.8
L_2	407	25.8	551	25.3	662	26.5
L_3	424	25.0	547	25.5	638	27.2
L_4	433	24.6	536	26.0	611	28.1
L_5	439	24.4	534	26.1	604	28.2
L_6	439	24.4	525	26.4	588	28.8
L_7	439	24.4	520	26.5	578	29.2
L_8	439	24.4	516	26.6	571	29.4
L_9	437	24.4	512	26.7	563	29.7
L_{10}	434	24.6	498	27.4	544	30.5
L_{11}	430	24.8	493	27.6	536	30.7
L_{12}	426	25.0	481	28.1	519	31.5
L_{13}	422	25.0	478	28.1	516	31.5
L_{14}	412	25.6	464	28.9	499	32.5
L_{15}	408	25.7	459	29.1	495	32.6

TABLE II (Continued)

RUN	40	41	42
G - lbm/hr-ft^2	110000	153800	154800
I - amps	200	222	207
E - volts	10.0	10.8	9.65
(q/A) - Btu/hr-ft^2	20400	24400	20400
P_i - psia	18.55	19.33	18.95
ΔP - psi	1.64	2.30	1.94
T_s - ^oR	143	144	143

Location	T_w-T_s (^oF)	h (Btu/hr-ft^2-^oF)	T_w-T_s (^oF)	h (Btu/hr-ft^2-^oF)	T_w-T_s (^oF)	h (Btu/hr-ft^2-^oF)
L_1	816	27.2	705	37.0	576	36.8
L_2	763	28.5	638	39.8	540	38.5
L_3	721	29.6	620	40.6	536	38.6
L_4	683	30.6	602	41.5	529	39.2
L_5	672	31.0	600	41.4	531	38.9
L_6	648	31.8	587	42.0	524	39.4
L_7	635	32.1	578	42.5	520	39.6
L_8	621	32.6	570	42.8	515	40.0
L_9	612	32.8	558	43.5	507	40.4
L_{10}	586	34.0	536	45.0	493	41.2
L_{11}	576	34.4	523	46.0	483	41.8
L_{12}	557	35.3	506	47.1	471	42.0
L_{13}	556	36.5	496	47.5	461	43.2
L_{14}	540	39.6	476	49.0	444	44.4
L_{15}	540	41.8	472	50.6	436	45.1

TABLE II (Continued)

RUN	43	44	45
G - lbm/hr-ft^2	156200	158000	164200
I - amps	191	174	154
E - volts	8.65	7.75	6.50
(q/A) - Btu/hr-ft^2	16800	13700	10150
P_i - psia	18.67	18.44	18.11
ΔP - psi	1.59	1.30	1.06
T_s - ^oR	143	143	143

Location	T_w-T_s (^oF)	h (Btu/hr-ft^2-^oF)	T_w-T_s (^oF)	h (Btu/hr-ft^2-^oF)	T_w-T_s (^oF)	h (Btu/hr-ft^2-^oF)
L_1	458	36.9	351	38.0	241	40.4
L_2	453	37.2	389	35.2	281	35.4
L_3	456	37.0	377	36.0	281	35.6
L_4	458	37.1	388	35.2	291	34.5
L_5	462	36.8	396	34.7	304	33.2
L_6	461	36.8	400	34.4	316	32.2
L_7	460	36.9	401	34.4	321	31.8
L_8	459	36.9	404	34.3	327	31.2
L_9	454	37.2	403	34.3	327	31.4
L_{10}	447	37.6	402	34.3	335	30.6
L_{11}	441	37.9	397	34.6	331	31.0
L_{12}	435	38.3	396	34.6	337	30.4
L_{13}	426	39.0	388	35.2	331	31.0
L_{14}	412	40.0	379	35.9	329	31.2
L_{15}	405	40.6	375	36.2	327	31.4

TABLE II (Continued)

RUN	46	47	48
G - lbm/hr-ft^2	167200	206000	221000
I - amps	139.5	141	160.5
E - volts	5.75	5.64	6.55
(q/A) - Btu/hr-ft^2	8130	8110	10700
P_i - psia	17.97	18.77	19.25
ΔP - psi	.93	1.16	1.39
T_s - ^oR	142	143	144

Location	T_w-T_s (^oF)	h (Btu/hr-ft^2-^oF)	T_w-T_s (^oF)	h (Btu/hr-ft^2-^oF)	T_w-T_s (^oF)	h (Btu/hr-ft^2-^oF)
L_1	198	39.2	181	43.5	205	50.4
L_2	218	36.0	191	41.5	225	46.4
L_3	232	34.2	207	38.7	251	42.4
L_4	239	33.4	211	38.0	249	42.6
L_5	249	32.3	212	38.0	247	43.0
L_6	265	30.7	227	35.6	258	41.3
L_7	269	30.4	279	30.1	261	41.0
L_8	278	29.4	239	34.1	269	39.3
L_9	278	29.4	238	34.3	269	40.0
L_{10}	292	28.1	251	32.7	280	38.4
L_{11}	287	28.7	246	33.4	275	39.1
L_{12}	297	27.8	260	31.6	287	37.6
L_{13}	290	28.5	251	32.8	279	38.7
L_{14}	292	28.3	256	32.2	280	38.6
L_{15}	292	28.3	256	32.3	280	38.6

TABLE II (Continued)

RUN	49	50	51
G - lbm/hr-ft^2	216000	211000	209000
I - amps	179.5	195.5	214
E - volts	7.55	8.45	9.35
(q/A) - Btu/hr-ft^2	13800	16800	20400
P_i - psia	19.43	19.67	20.06
ΔP - psi	1.62	1.88	2.22
T_s - ^oR	144	144	144

Location	T_w-T_s (^oF)	h (Btu/hr-ft^2-^oF)	T_w-T_s (^oF)	h (Btu/hr-ft^2-^oF)	T_w-T_s (^oF)	h (Btu/hr-ft^2-^oF)
L_1	250	53.0	311	52.4	345	57.4
L_2	291	46.8	390	44.0	434	48.0
L_3	325	42.6	365	46.4	402	50.7
L_4	303	45.1	357	46.9	390	52.1
L_5	307	44.6	365	46.1	400	51.0
L_6	315	43.7	370	45.6	407	50.4
L_7	320	43.2	373	45.3	411	50.0
L_8	327	42.4	378	44.9	415	49.5
L_9	326	42.6	376	45.1	413	49.9
L_{10}	334	41.7	377	44.9	412	49.9
L_{11}	330	42.2	373	45.3	408	50.3
L_{12}	335	41.5	373	45.2	403	50.8
L_{13}	328	42.3	365	46.1	394	51.8
L_{14}	324	42.8	355	47.3	381	53.3
L_{15}	322	43.0	351	47.6	375	53.9

TABLE II (Continued)

RUN	52	53	54
G - lbm/hr-ft^2	206000	205000	70000
I - amps	233	249	160
E - volts	10.6	11.5	8.73
(q/A) - Btu/hr-ft^2	25200	29200	14200
P_i - psia	20.50	20.95	17.91
ΔP - psi	2.67	3.10	.97
T_s - ^oR	143	145	142

Location	T_w-T_s (^oF)	h (Btu/hr-ft^2-^oF)	T_w-T_s (^oF)	h (Btu/hr-ft^2-^oF)	T_w-T_s (^oF)	h (Btu/hr-ft^2-^oF)
L_1	423	58.7	502	58.2	770	19.2
L_2	527	49.7	597	51.4	785	19.0
L_3	452	55.9	513	57.3	762	19.4
L_4	449	56.3	509	57.9	731	19.8
L_5	461	54.9	519	56.9	724	20.0
L_6	464	54.6	519	56.9	701	20.4
L_7	465	54.6	519	56.9	687	20.7
L_8	468	54.3	517	56.7	672	21.0
L_9	463	54.7	509	57.5	667	21.2
L_{10}	455	55.5	493	59.1	645	21.6
L_{11}	448	56.1	484	60.0	640	21.7
L_{12}	438	57.3	469	61.5	624	23.0
L_{13}	428	58.2	459	62.4	630	24.0
L_{14}	410	60.3	438	64.6	621	25.6
L_{15}	402	61.0	430	65.5	624	27.0

TABLE II (Continued)

RUN	55	56	57
G - lbm/hr-ft^2	69800	69800	109600
I - amps	171	177.5	195
E - volts	9.47	10.0	10.28
(q/A) - Btu/hr-ft^2	16500	18100	20400
P_i - psia	18.00	18.02	18.86
ΔP - psi	1.12	1.31	1.74
T_s - ^oR	142	143	143

Location	T_w-T_s (^oF)	h (Btu/hr-ft^2-^oF)	T_w-T_s (^oF)	h (Btu/hr-ft^2-^oF)	T_w-T_s (^oF)	h (Btu/hr-ft^2-^oF)
L_1	888	19.8	974	20.2	742	28.8
L_2	884	19.9	945	20.4	753	28.7
L_3	837	20.6	892	21.2	729	29.2
L_4	795	21.2	844	21.9	698	30.1
L_5	780	21.5	823	22.3	688	30.4
L_6	750	22.1	787	22.9	662	31.1
L_7	734	22.4	767	23.3	645	31.6
L_8	715	22.8	748	23.7	635	32.1
L_9	710	23.0	744	24.0	622	32.5
L_{10}	686	23.9	719	26.0	597	33.5
L_{11}	683	25.3	719	27.5	587	33.9
L_{12}	669	27.0	710	29.6	565	34.8
L_{13}	682	28.3	729	30.8	567	36.0
L_{14}	678	30.4	729	33.2	552	38.4
L_{15}	686	32.2	746	34.9	556	40.5

TABLE II (Continued)

RUN	58	59	60
G - lbm/hr-ft^2	110000	110000	156800
I - amps	205	214.5	190.5
E - volts	10.92	11.62	9.17
(q/A) - Btu/hr-ft^2	22800	25400	17800
P_i - psia	19.40	19.62	19.17
ΔP - psi	2.18	2.44	1.84
T_s - ^oR	144	144	143

Location	T_w-T_s (^oF)	h (Btu/hr-ft^2-^oF)	T_w-T_s (^oF)	h (Btu/hr-ft^2-^oF)	T_w-T_s (^oF)	h (Btu/hr-ft^2-^oF)
L_1	828	29.5	912	30.4	513	35.3
L_2	812	29.8	866	31.4	508	35.4
L_3	774	30.8	821	32.4	513	35.3
L_4	737	31.8	780	33.6	509	35.4
L_5	724	32.2	765	34.0	508	35.4
L_6	695	33.1	730	35.0	501	35.8
L_7	676	33.7	707	35.6	498	36.0
L_8	662	34.3	691	36.2	496	36.0
L_9	647	34.8	676	36.8	487	36.5
L_{10}	620	35.8	648	38.2	475	37.3
L_{11}	610	36.2	640	40.3	466	37.8
L_{12}	587	39.0	620	44.2	455	38.4
L_{13}	594	40.8	634	45.9	446	39.0
L_{14}	582	44.0	629	49.5	430	40.2
L_{15}	593	46.4	650	51.8	423	40.7

TABLE II (Continued)

RUN	61	62
G - lbm/hr-ft^2	154900	154500
I - amps	221.5	225
E - volts	11.22	11.54
(q/A) - Btu/hr-ft^2	25300	26500
P_i - psia	20.09	20.17
ΔP - psi	2.69	2.80
T_s - ^oR	144	144

Location	T_w-T_s (^oF)	h (Btu/hr-ft^2-^oF)	T_w-T_s (^oF)	h (Btu/hr-ft^2-^oF)
L_1	674	39.4	702	39.8
L_2	662	39.8	687	40.3
L_3	650	40.3	672	40.9
L_4	634	41.0	654	41.8
L_5	632	41.1	650	47.9
L_6	613	42.0	630	42.9
L_7	601	42.5	617	43.4
L_8	592	42.9	606	43.9
L_9	576	43.7	590	44.7
L_{10}	550	45.3	562	46.3
L_{11}	536	46.0	546	47.2
L_{12}	513	47.5	523	48.8
L_{13}	507	48.0	520	49.0
L_{14}	488	49.4	501	52.0
L_{15}	487	52.1	502	54.7

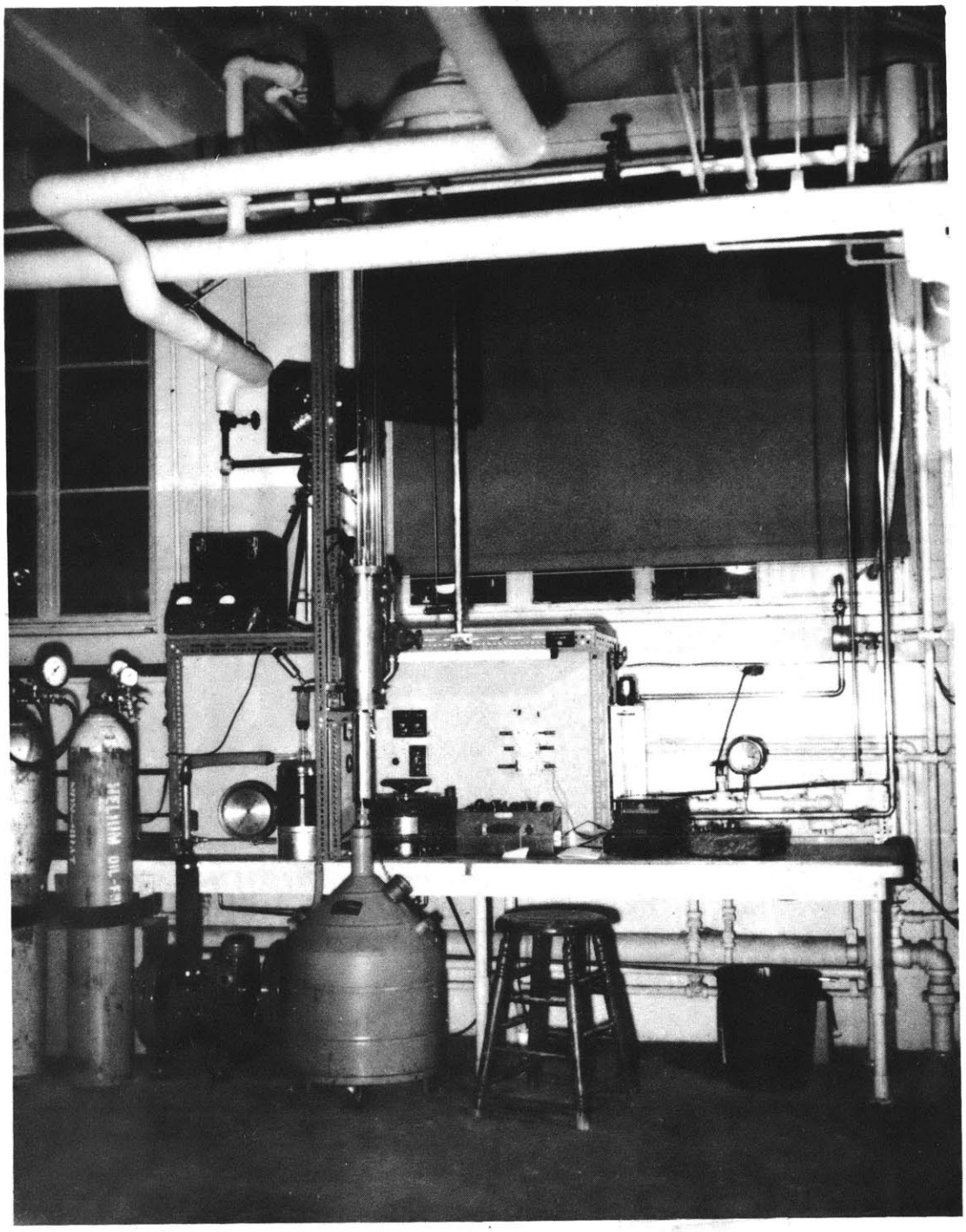

Fig. 1 Photograph of the Nitrogen Film Boiling Test Apparatus

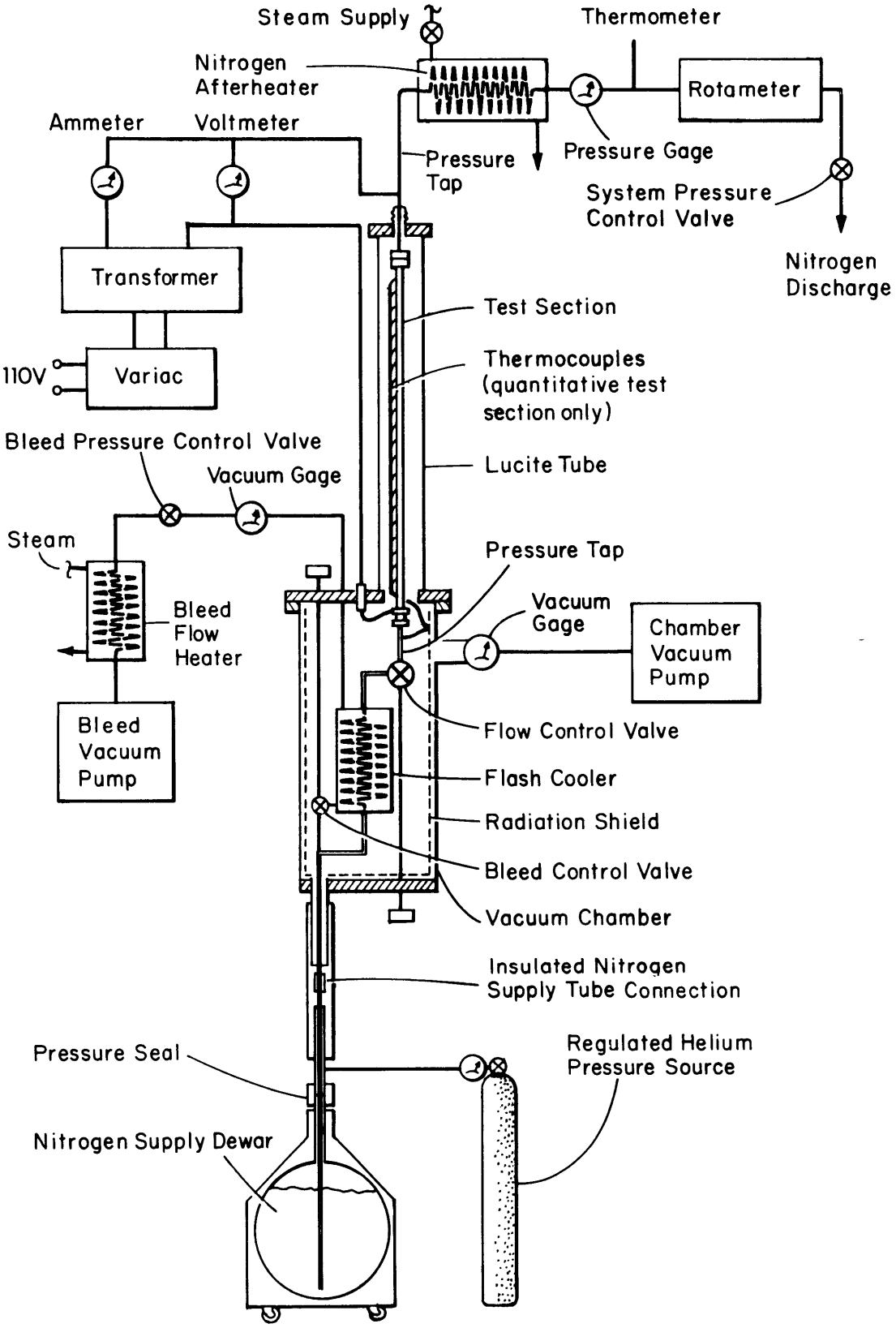

FIGURE 2 SCHEMATIC DIAGRAM OF THE NITROGEN FILM BOILING TEST APPARATUS.

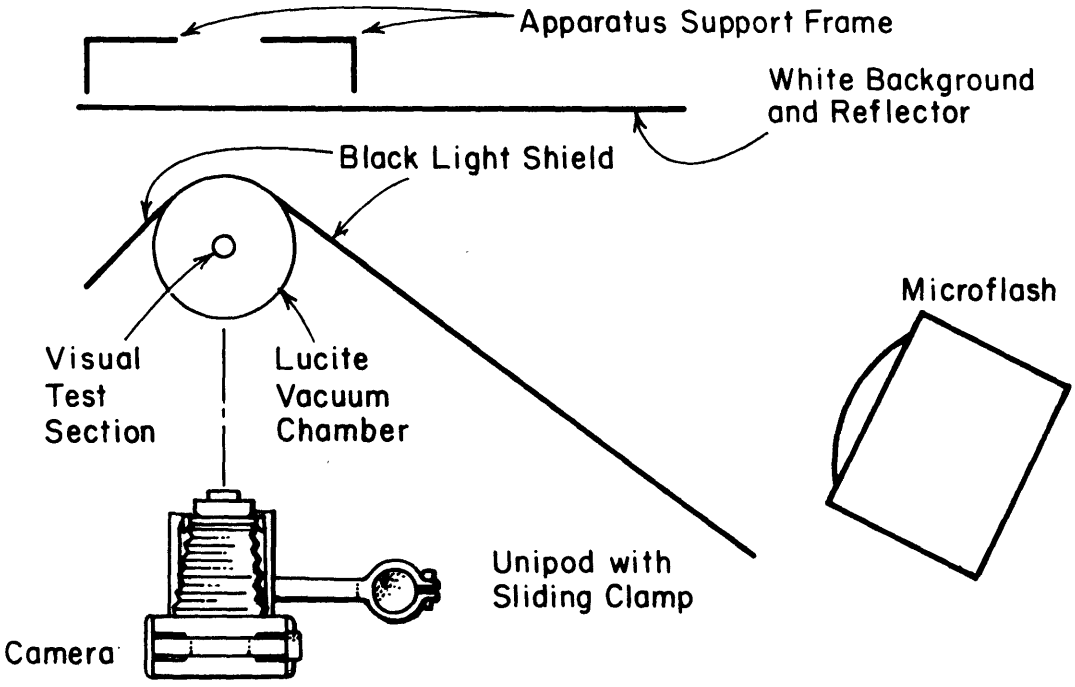

a) Layout with White Background.

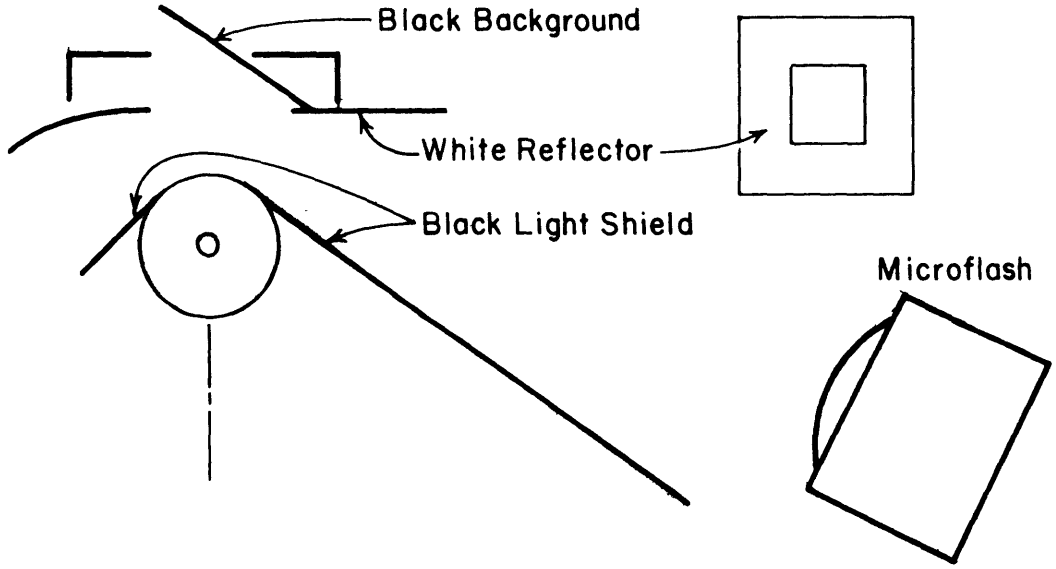

b) Arrangement of Black Background

Figure 3 Schematic Plan View of the Photographic Layout.

a) Vapor Quality Range:
0% to 6%

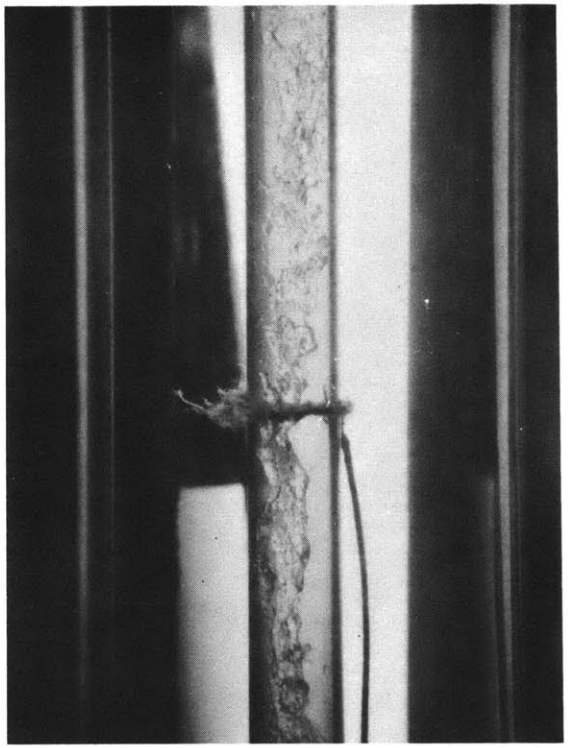

b) Vapor Quality Range
5% to 11%

Fig. 4 Film Boiling Inside a Vertical Tube

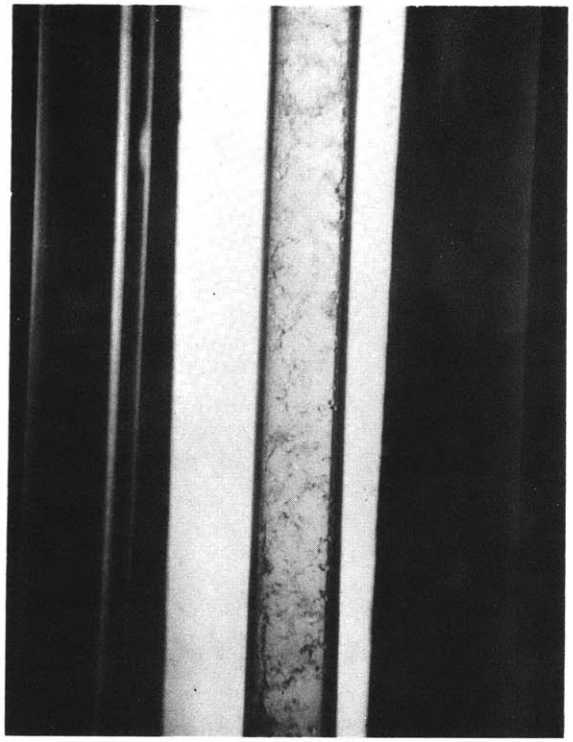

a) Vapor Quality Range:
34% to 41%

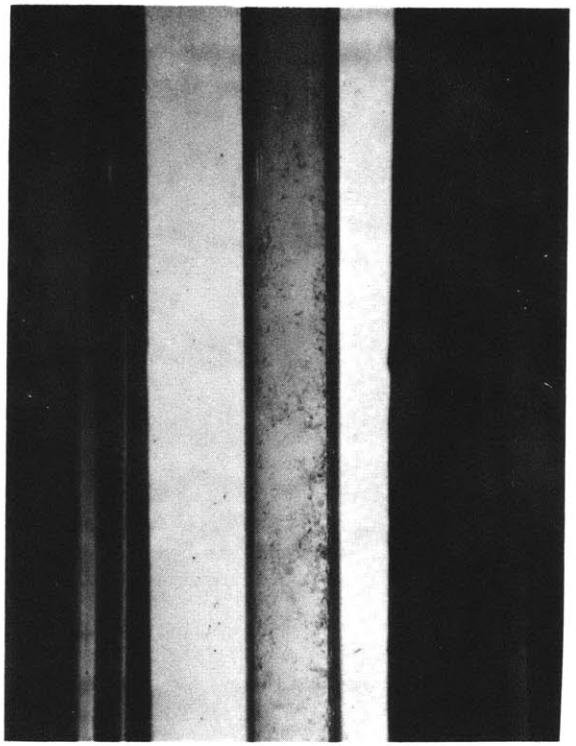

b) Vapor Quality Range:
43% to 50%

Fig. 5 Film Boiling Inside a Vertical Tube

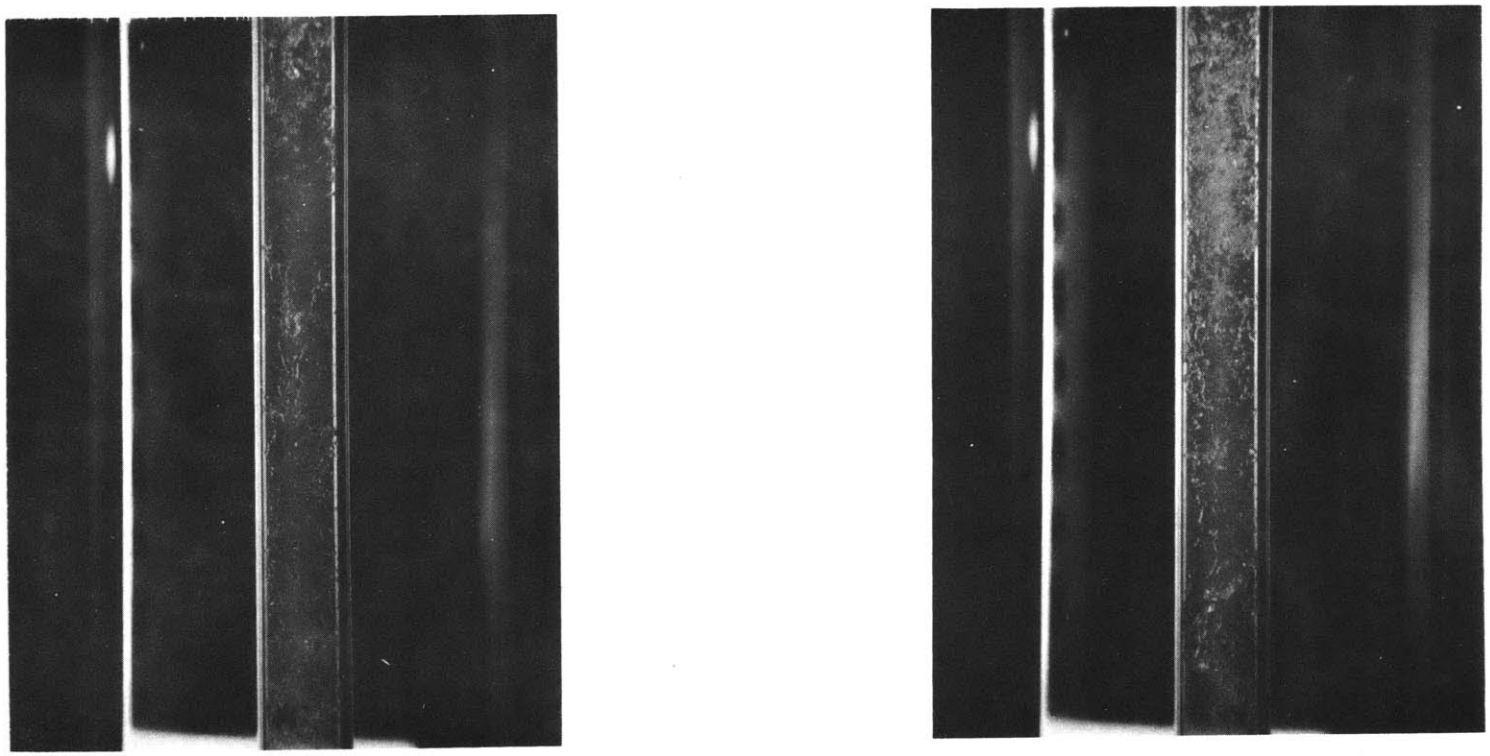

Vapor Quality Range: 34% to 41%

Fig. 6 Film Boiling Inside a Vertical Tube

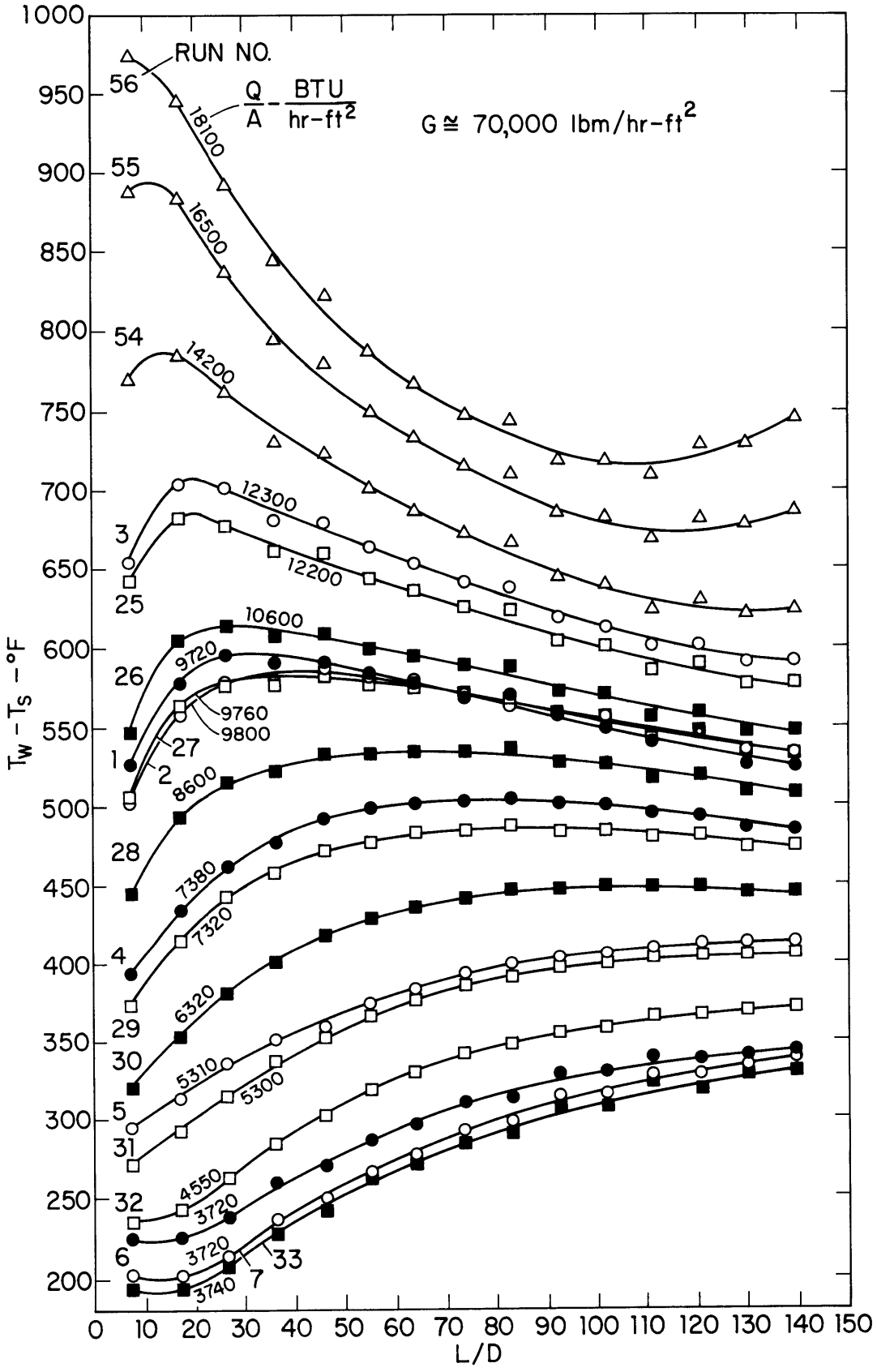

FIGURE 7 WALL SUPERHEAT VARIATION ALONG THE TUBE

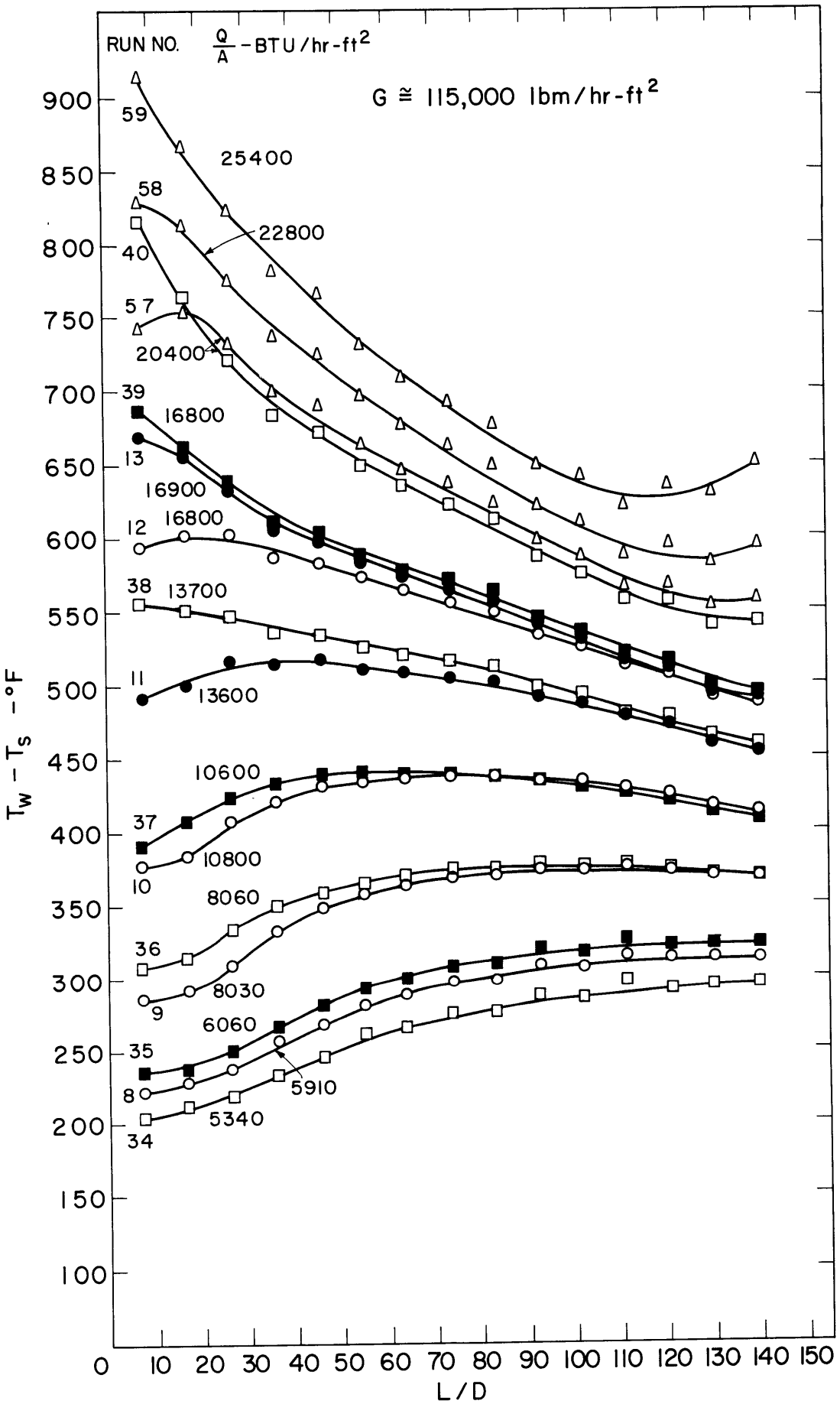

FIGURE 8 WALL SUPERHEAT VARIATION ALONG THE TUBE

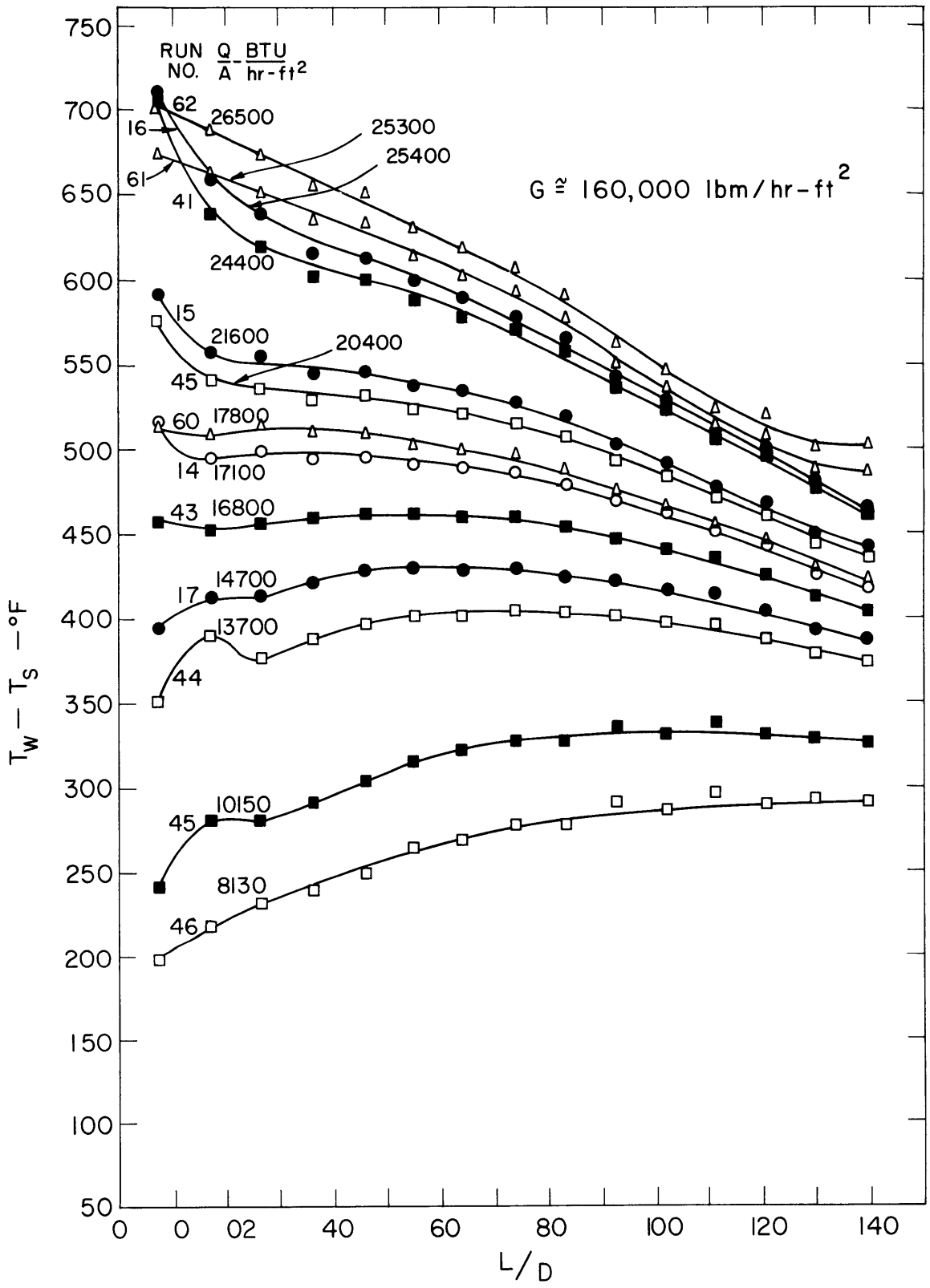

FIGURE 9 WALL SUPERHEAT VARIATION ALONG THE TUBE

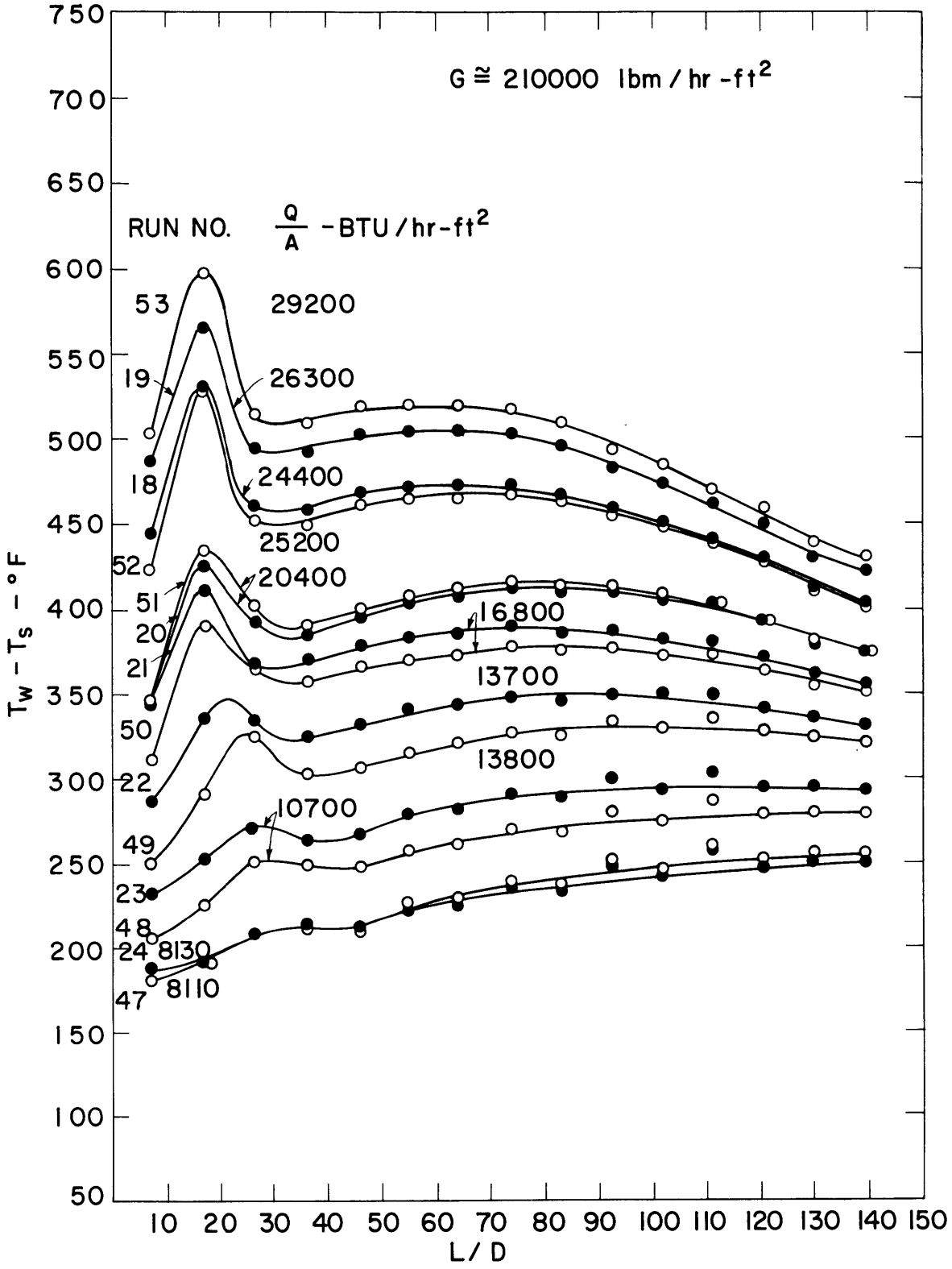

FIGURE 10 WALL SUPERHEAT VARIATION ALONG THE TUBE

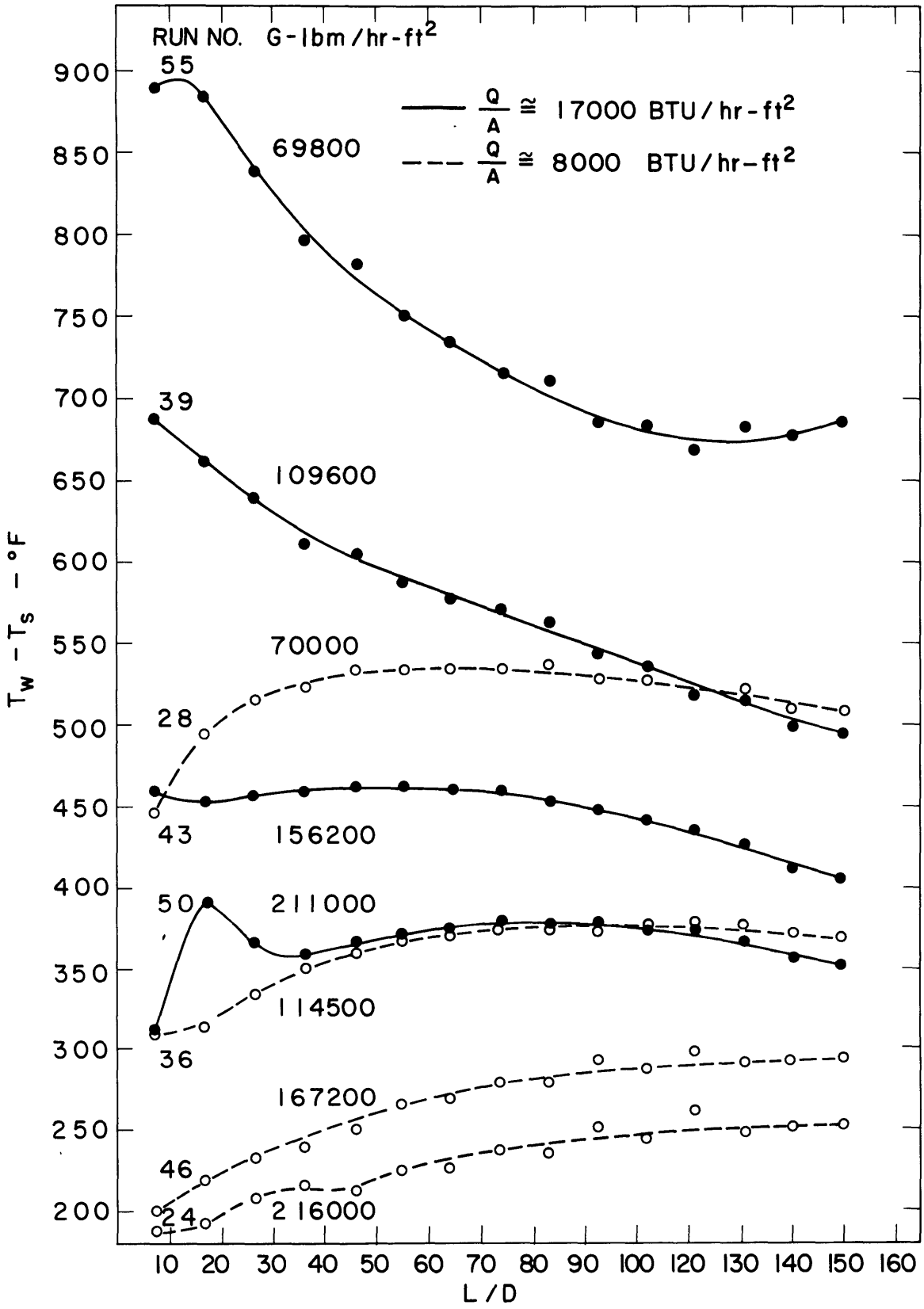

FIGURE 11 EFFECT OF FLOW RATE ON WALL SUPERHEAT VARIATION ALONG THE TUBE

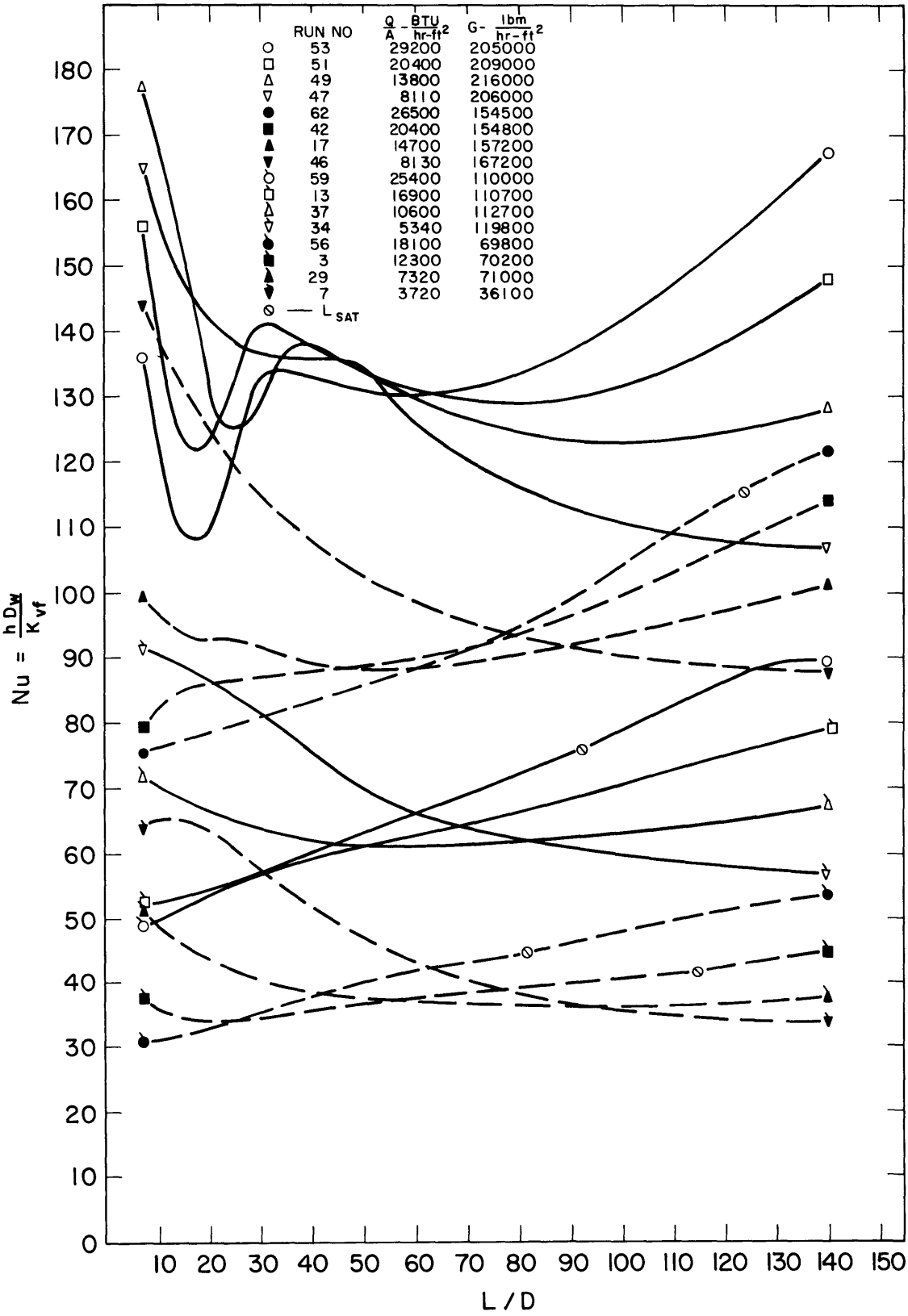

FIGURE 12 TYPICAL NUSSELT NUMBER VARIATION ALONG THE TUBE.

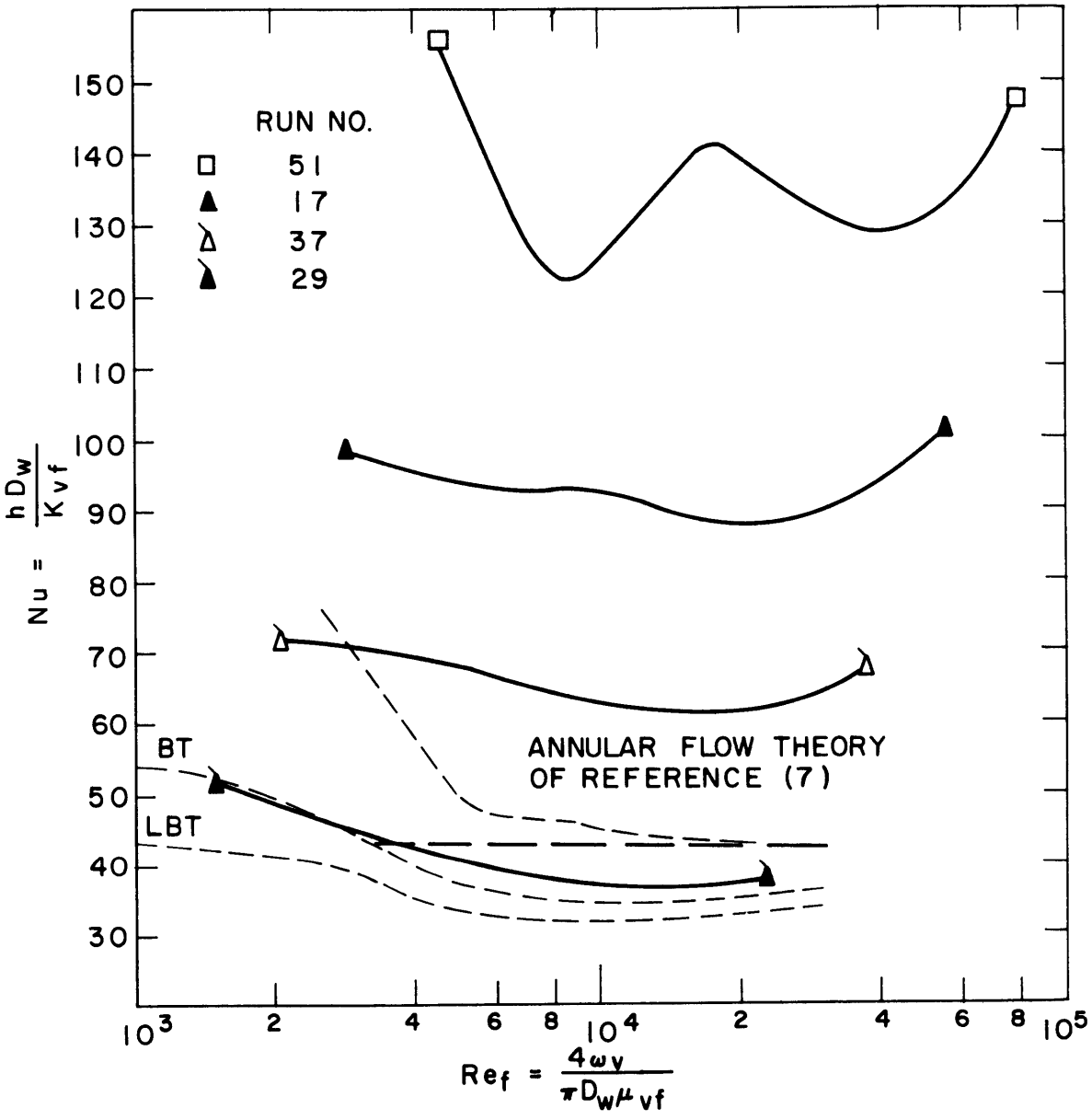

FIGURE 13 COMPARISON OF NITROGEN FILM BOILING DATA WITH THE ANNULAR FLOW THEORY OF REFERENCE (7)

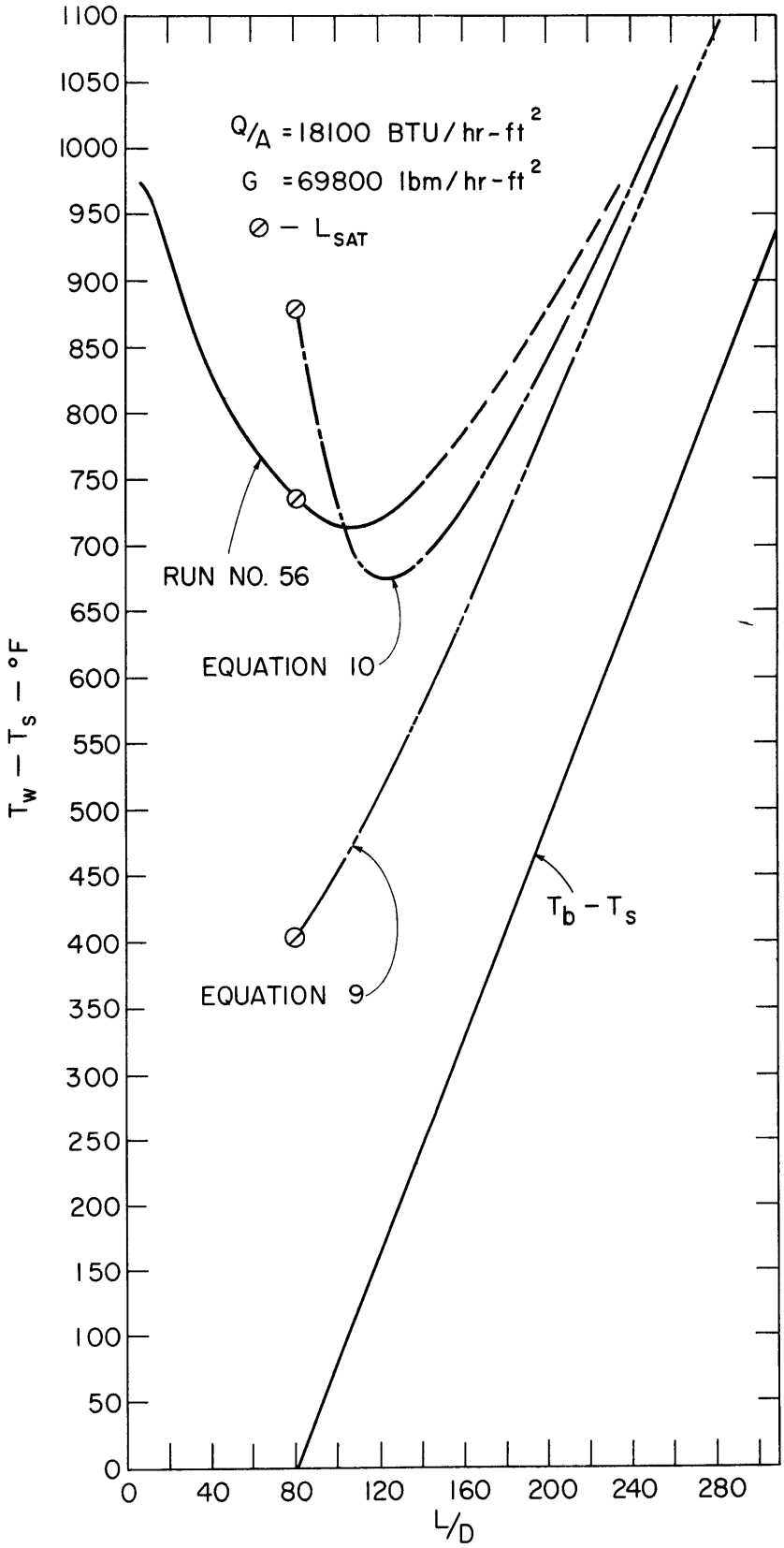

FIGURE 14 EFFECT OF PROPERTY EVALUATION ON THE DITTUS - BOELTER EQUATION

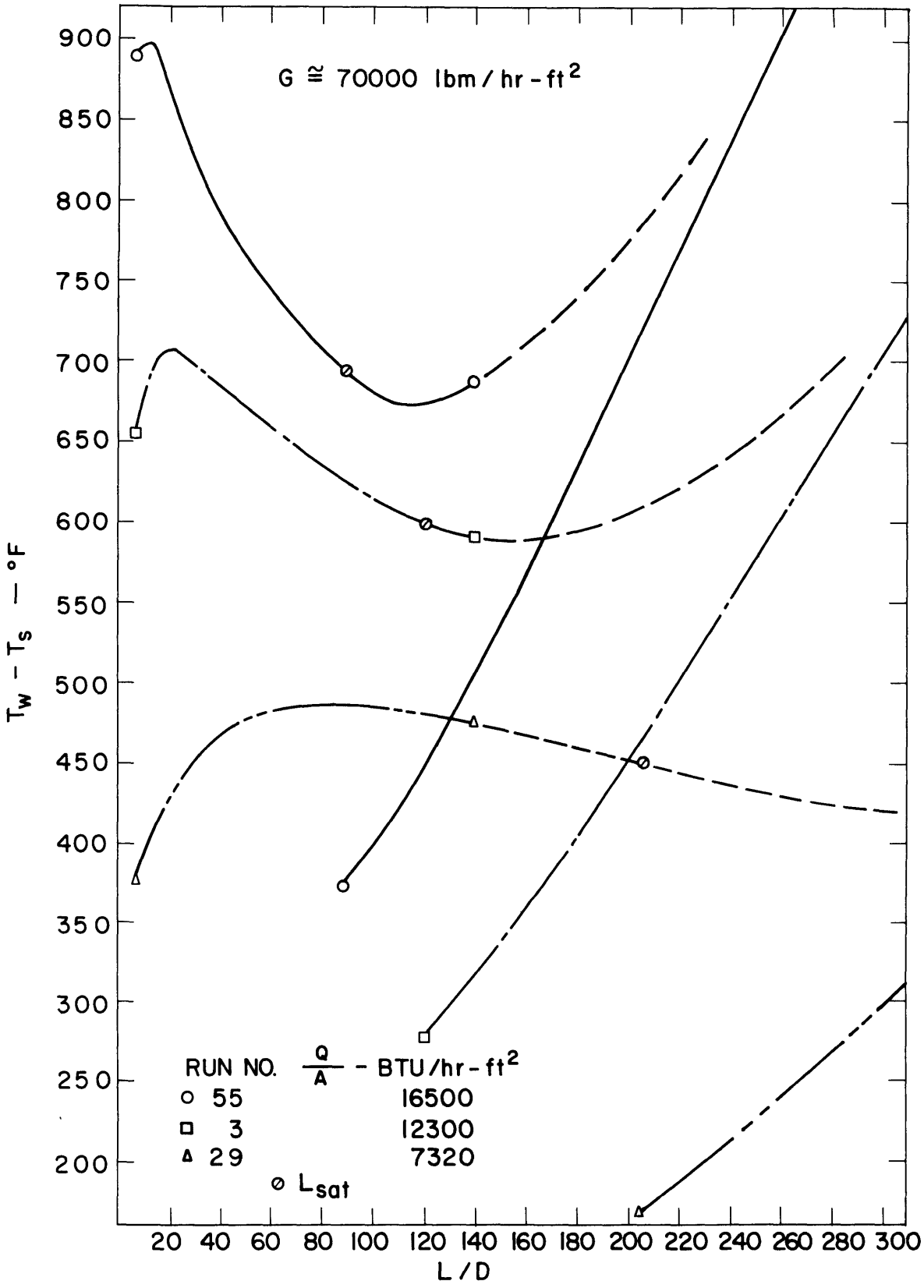

FIGURE 15 EXTRAPOLÁTION OF THE DATA TOWARD THE PURE VAPOR STATE

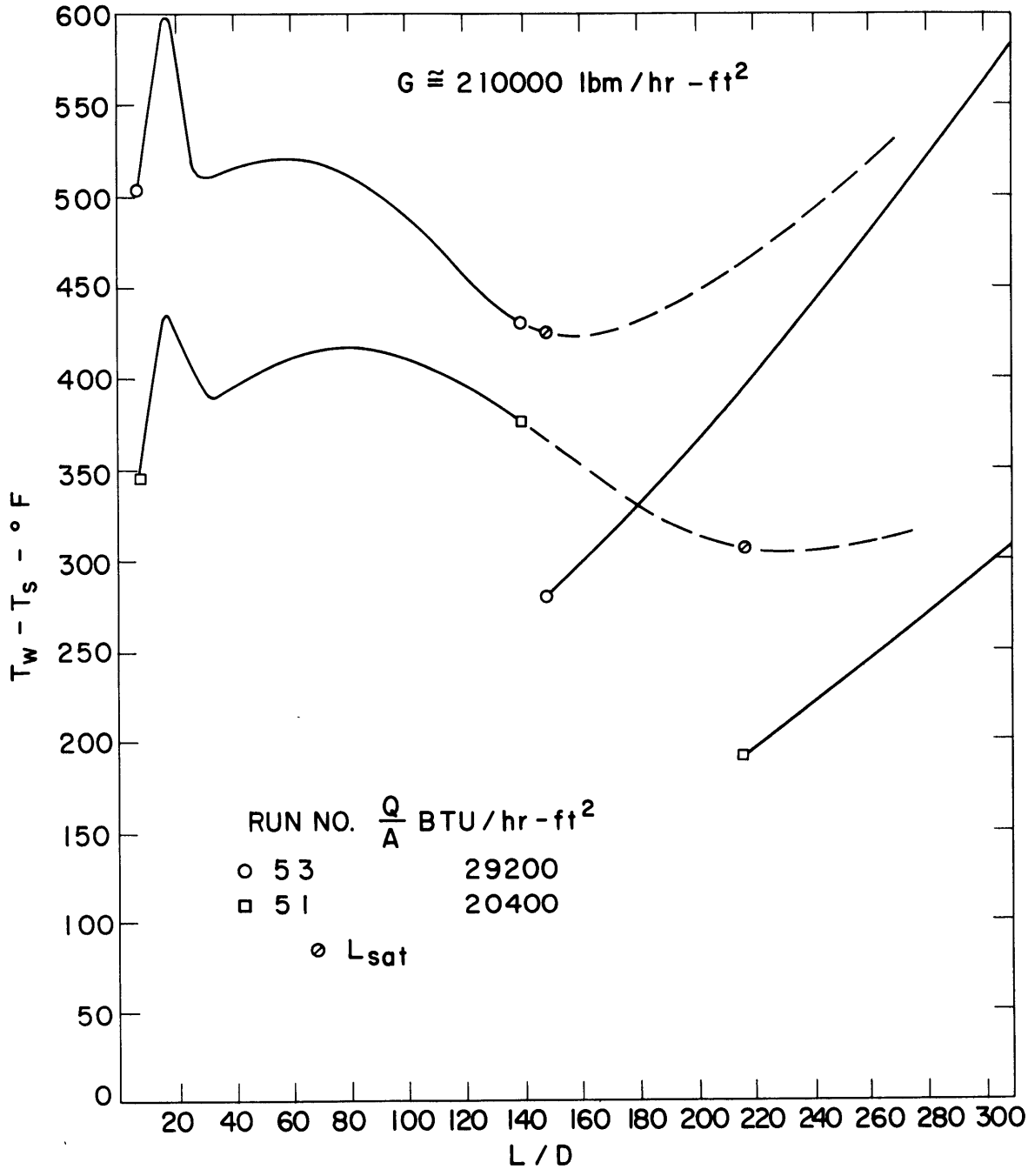

FIGURE 16 EXTRAPOLATION OF THE DATA TOWARD THE PURE VAPOR STATE

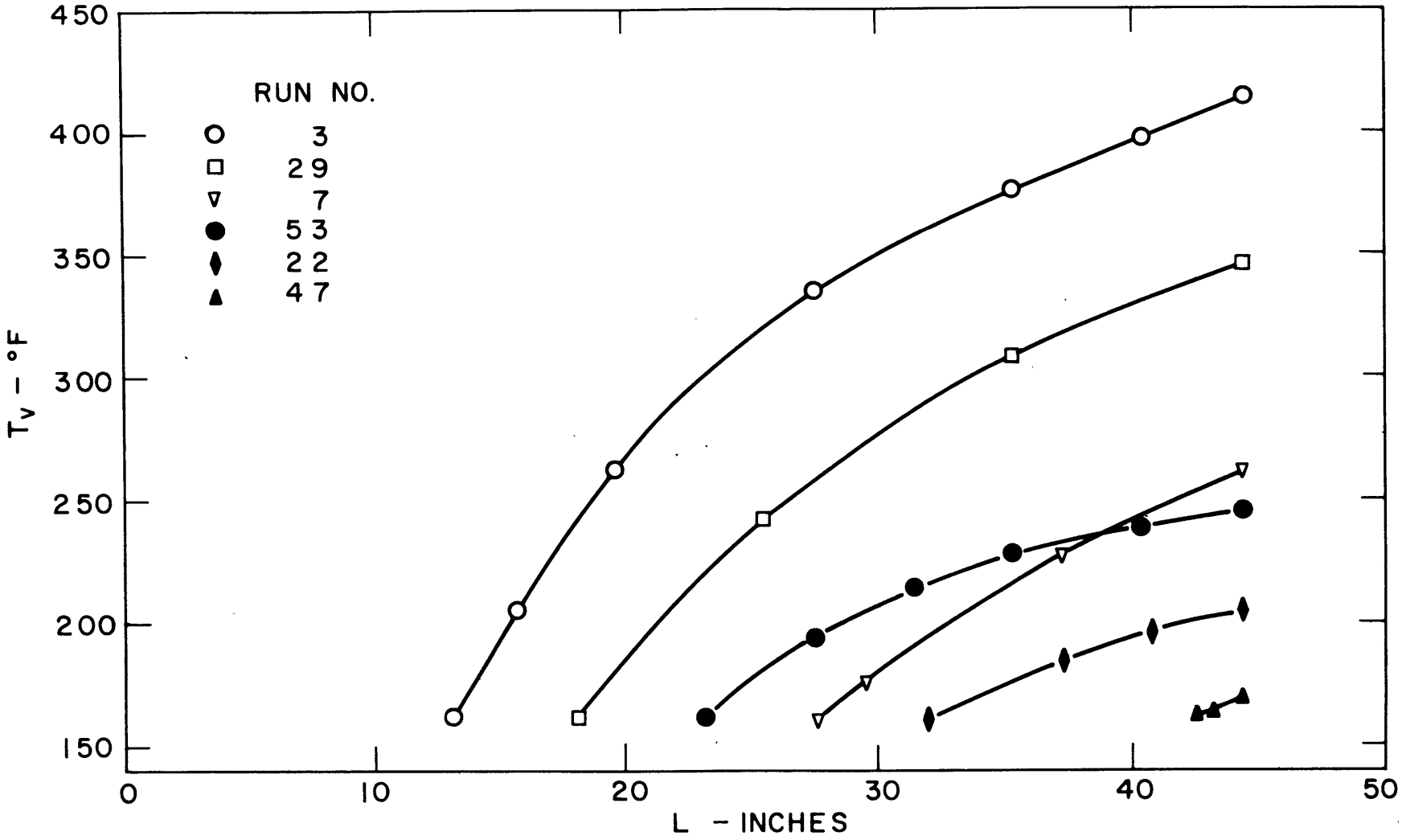

FIGURE 17 CALCULATED VAPOR TEMPERATURE

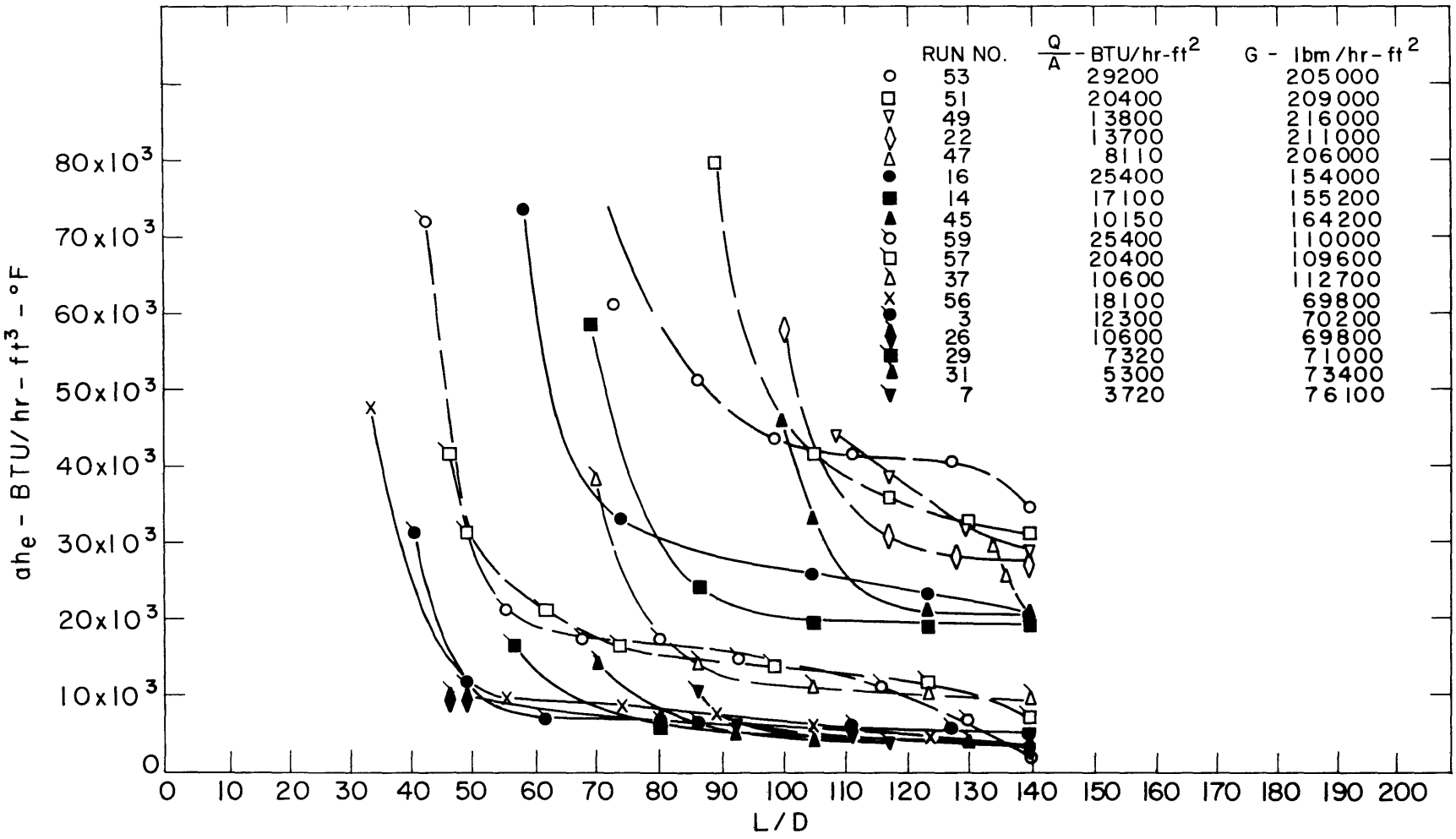

FIGURE 18 VARIATION OF THE VOLUME EVAPORATION COEFFICIENT, ah_e, ALONG THE TUBE

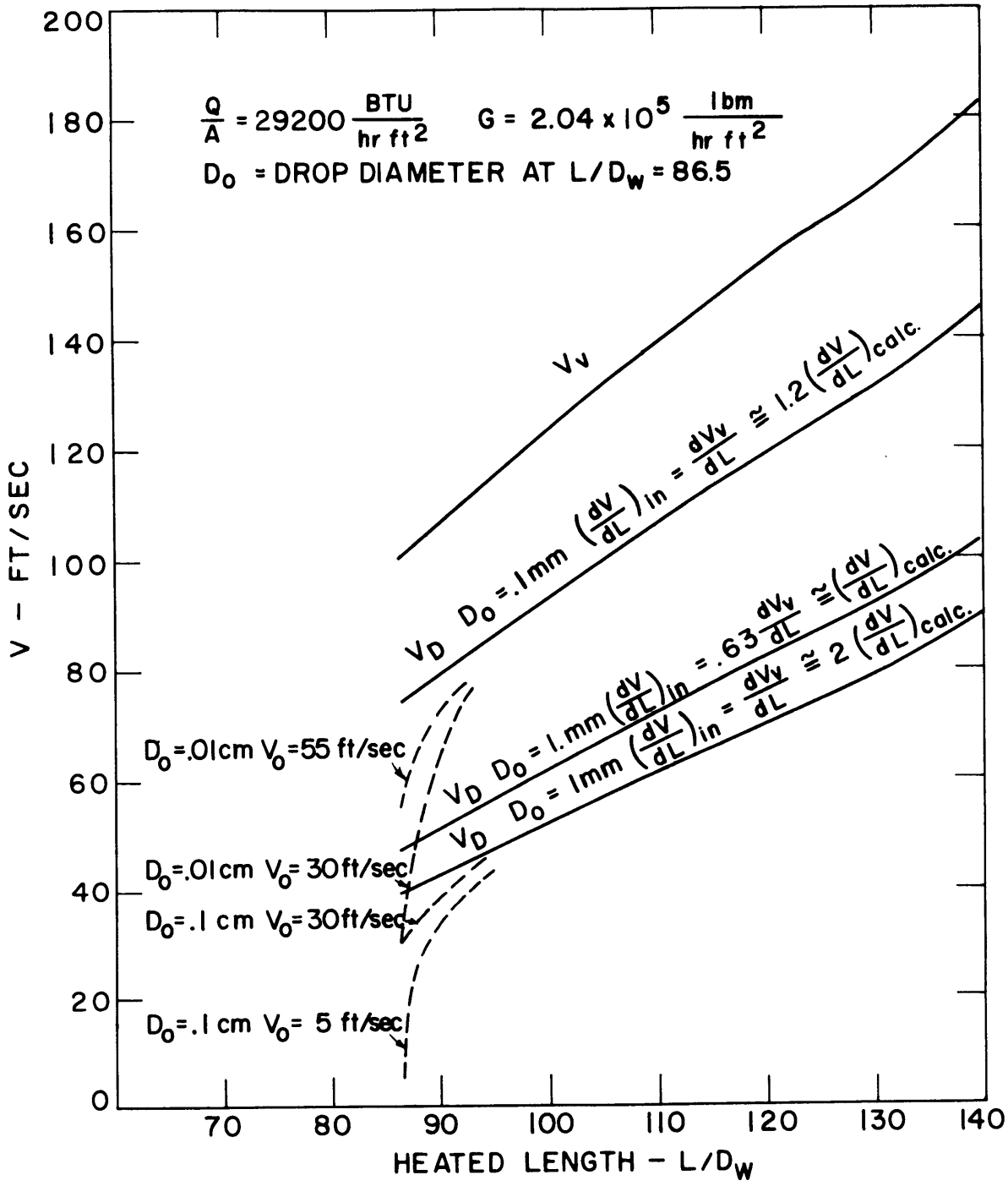

FIGURE 19 DROPLET ACCELERATION ANALYSIS

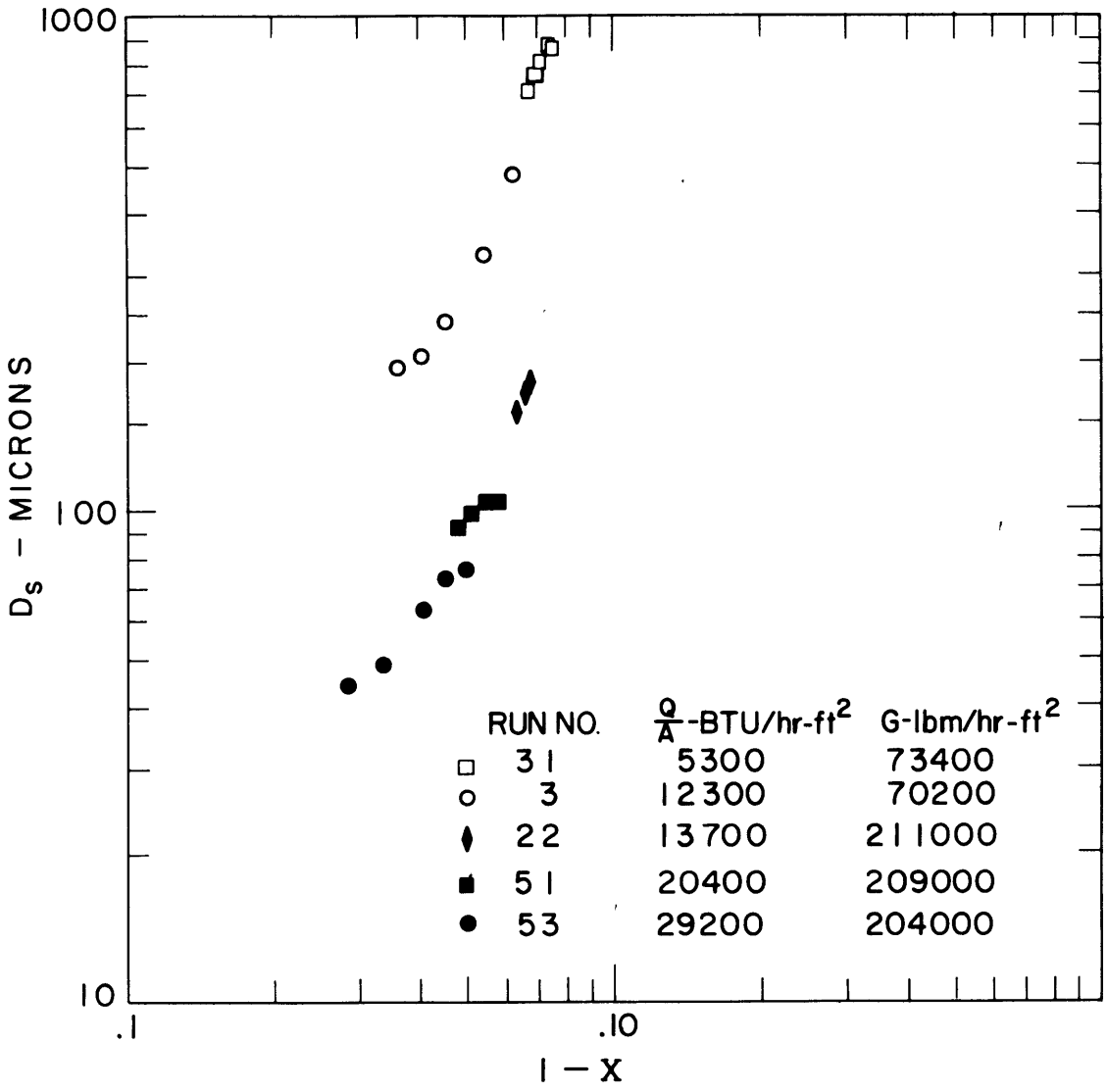

FIGURE 20 CALCULATED MEAN EFFECTIVE DROP SIZE

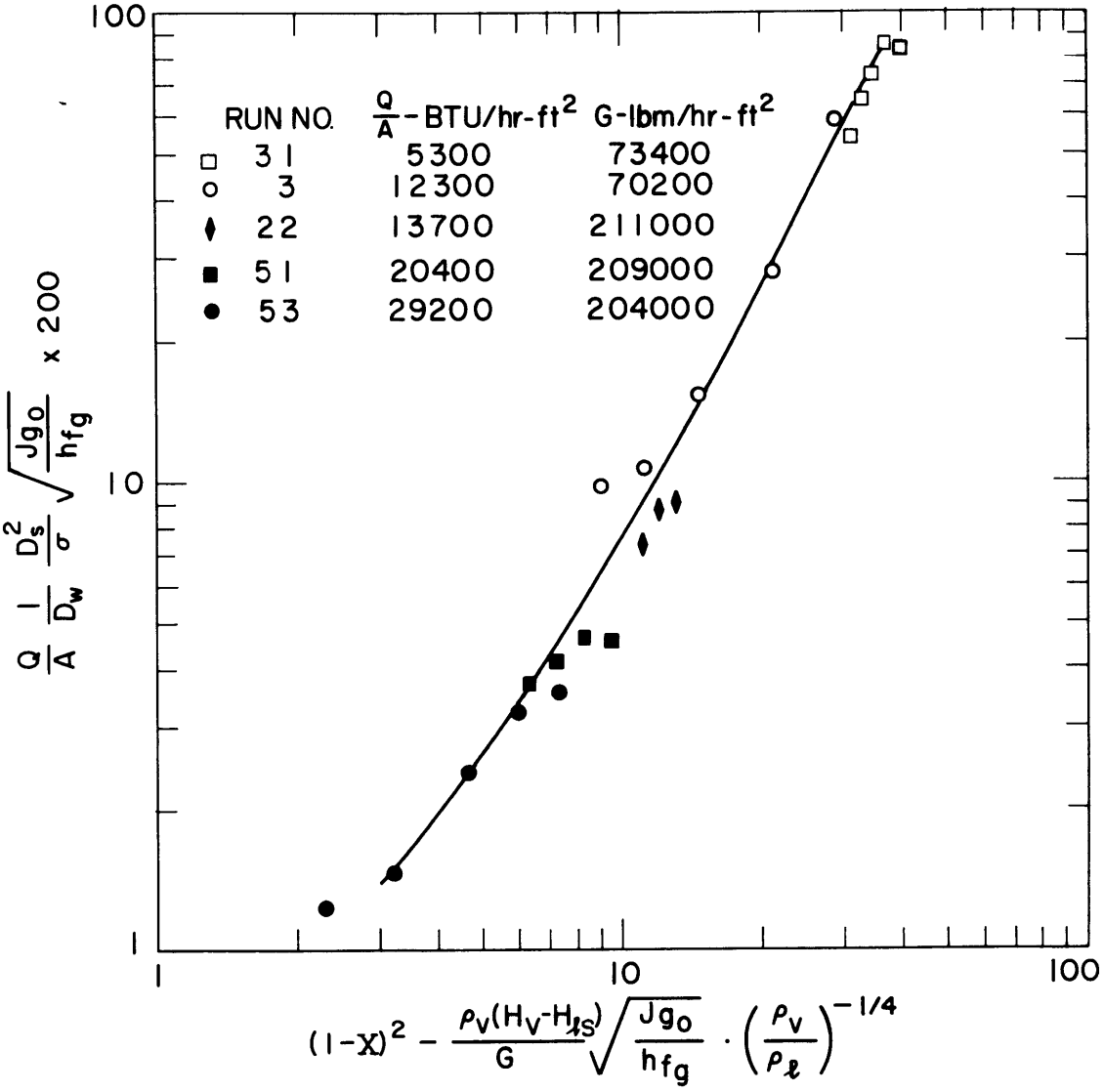

FIGURE 21 DROP SIZE CORRELATION

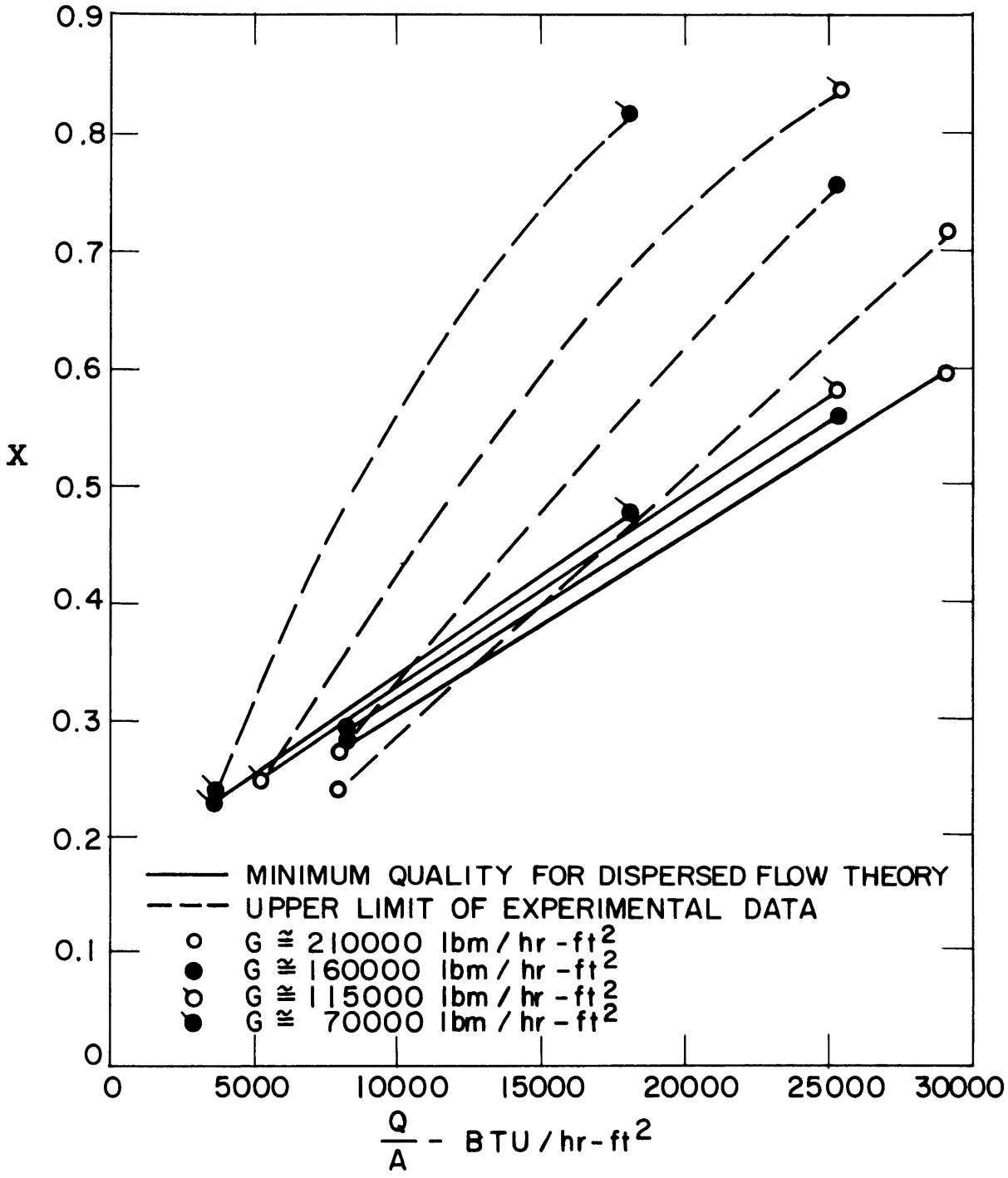

FIGURE 22 REGION OF VALIDITY OF THE DISPERSED FLOW THEORY

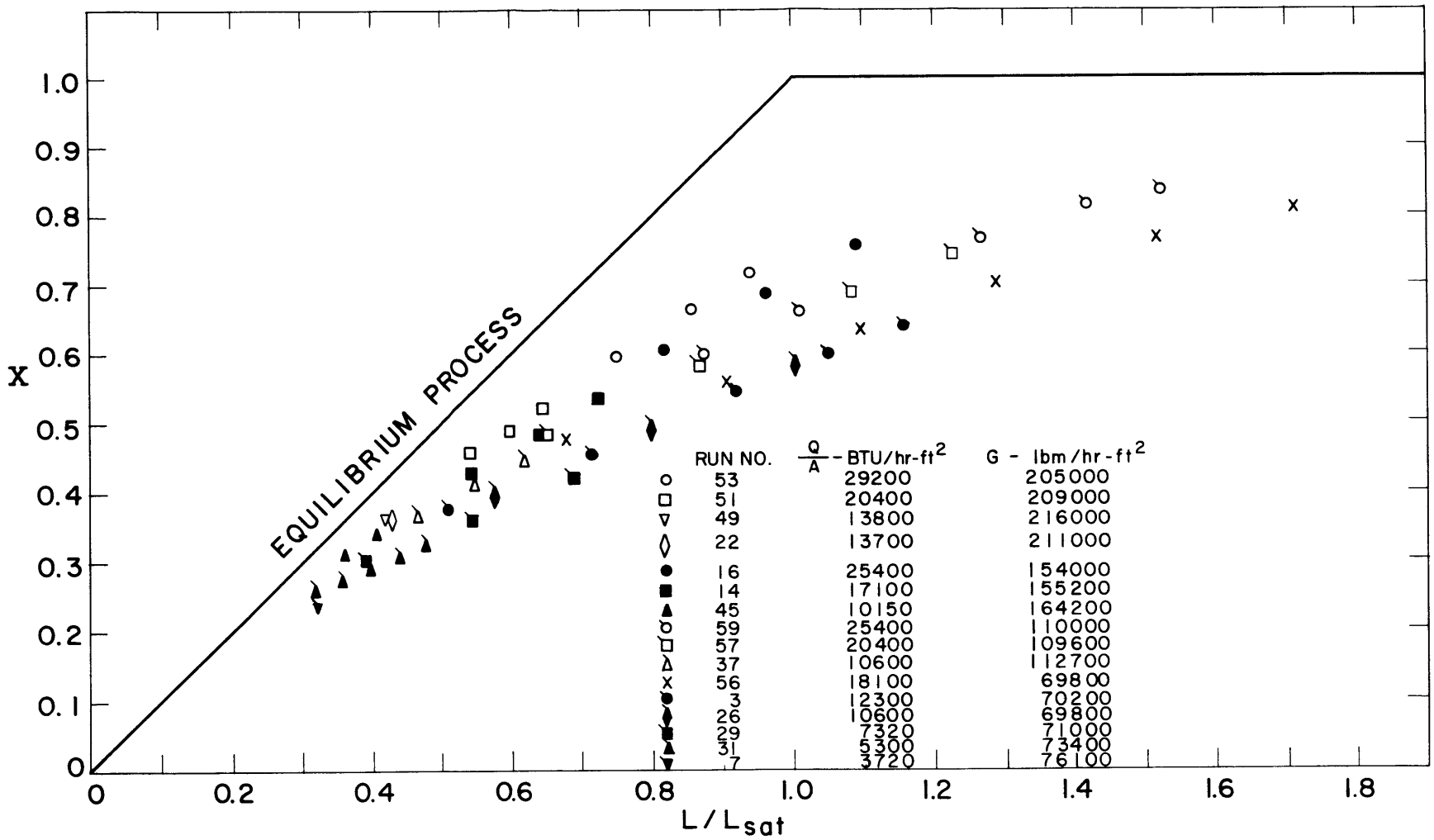

FIGURE 23 DISPLACEMENT OF THE FILM BOILING PROCESS FROM AN EQUILIBRIUM CONDITION

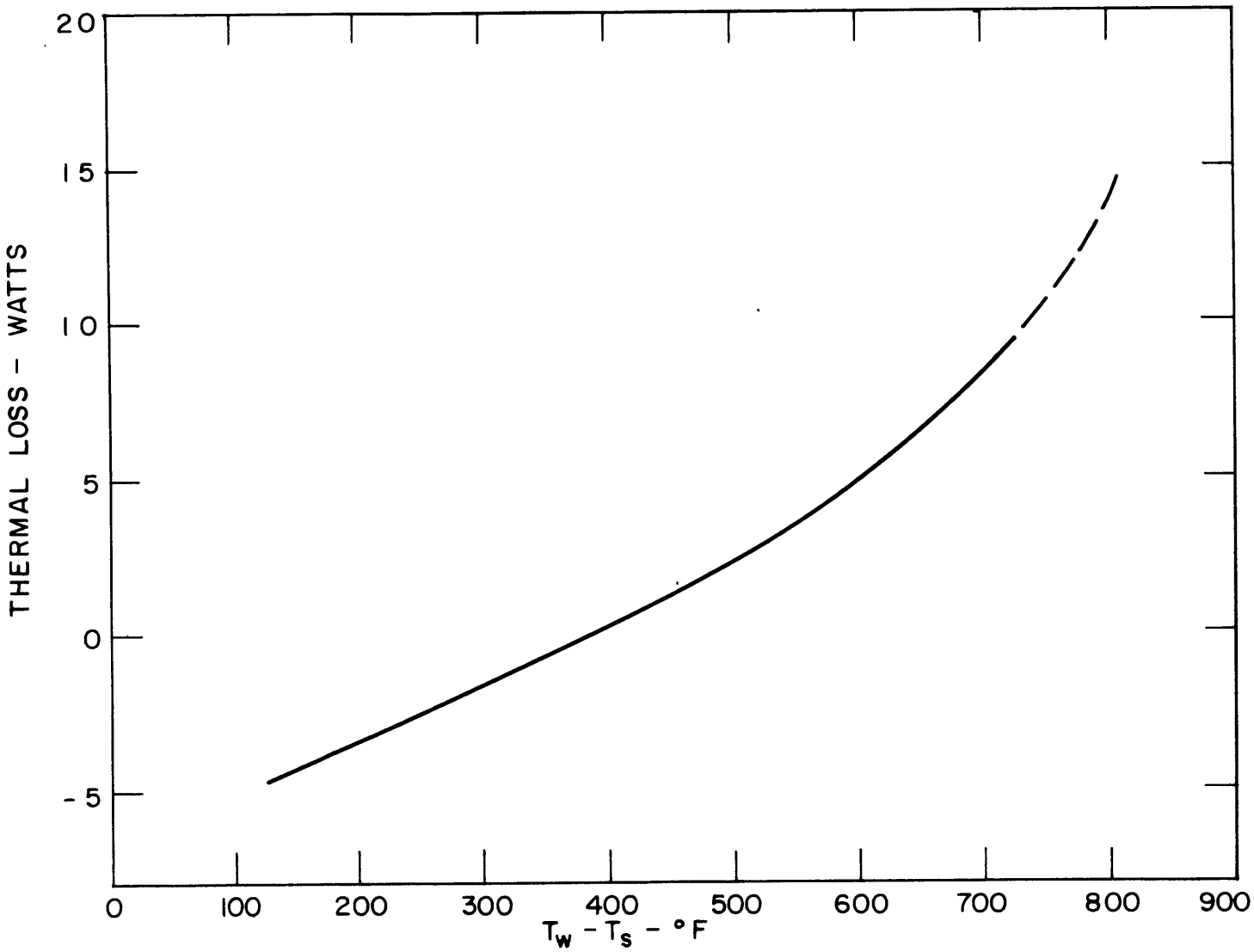

FIGURE 24 THERMAL LOSSES FROM THE OUTER SURFACE OF THE TEST SECTION

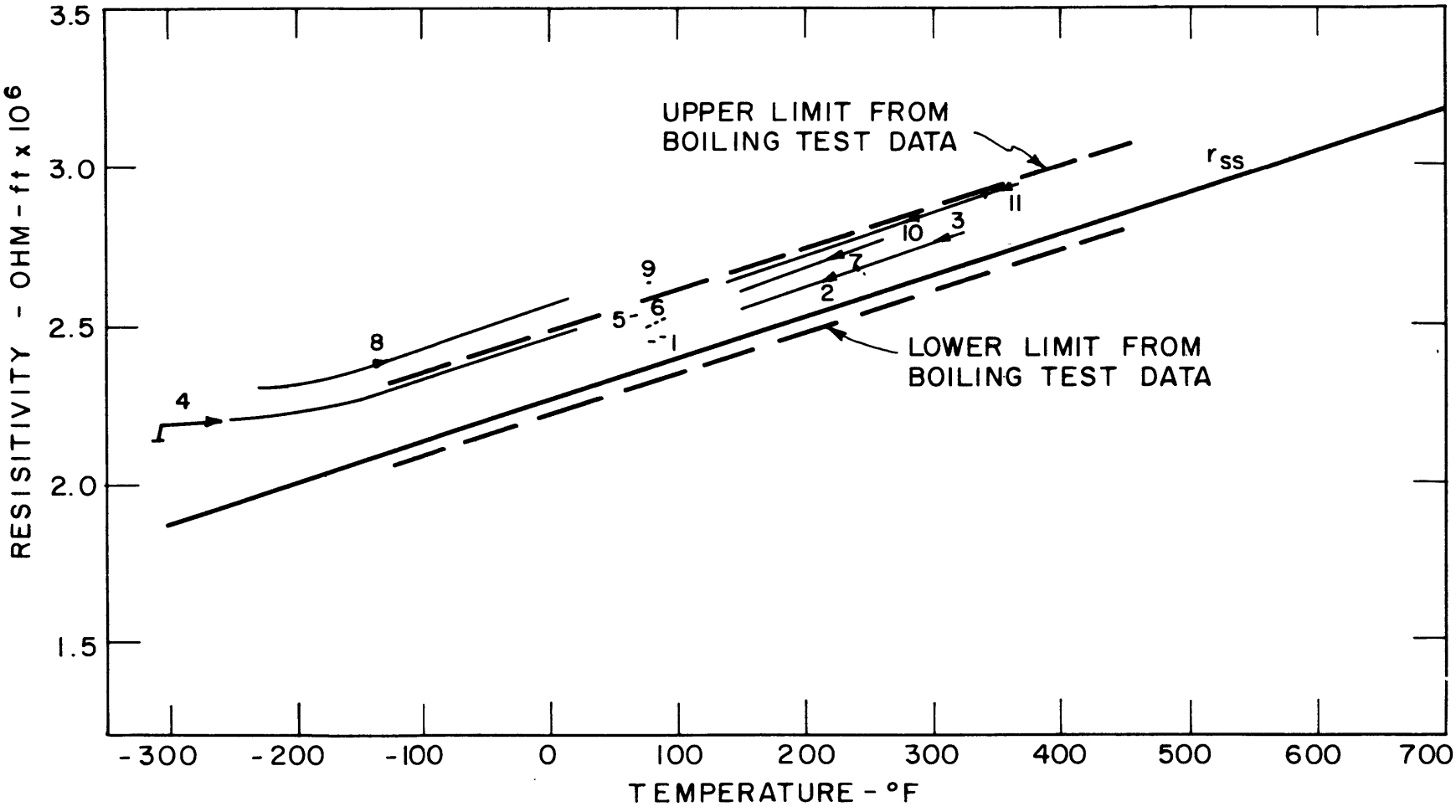

FIGURE 25 ELECTRICAL RESISTIVITY OF THE 304 STAINLESS STEEL TEST SECTION